A LABORATORY INVESTIGATION OF THE THERMOELECTRIC EFFECT IN CLEAN SILICA SANDS

by

Clinton Meyer

A thesis submitted to the Faculty and the Board of Trustees of the Colorado School of Mines in partial fulfillment of the requirements for the degree of Masters of Science (Hydrological Science and Engineering Program through the department of Geophysics).

Golden, Colorado

Date: _____

Signed: _____

Clinton Meyer

Signed: _____

Dr. André Revil

Thesis Advisor

Golden, Colorado

Date: _____

Signed: _____

Dr. Terri Hogue

Professor and Head

Hydrological Science and Engineering Program

ABSTRACT

The effect of thermoelectric coupling on self-potential was investigated by applying a temperature gradient to unconsolidated sands fully saturated by saline (NaCl) solutions. Thus far, very few published investigations have taken into account the effect of temperature on the electrodes and the ionic strength of the pore water, generating spurious diffusion potentials typically on the same order of magnitude as the thermoelectric effect. For this investigation, 25 experiments are conducted to test the influence of salinity upon the thermoelectric coupling coefficient over four orders of magnitude in salinity variation. The intrinsic thermoelectric coefficient ranged from -0.4 mV $°C^{-1}$ (10^{-3} M NaCl) to +0.9 mV $°C^{-1}$ at very low salinities (10^{-4} M). Silica sands with median grain sizes of 0.72 mm and 0.2 mm were used, with corresponding surface conductivities of 1.52×10^{-5} (S m^{-1}) and 5.43×10^{-5} (S m^{-1}), respectively. In order to isolate the thermoelectric response associated with the temperature gradient, raw self-potential measurements were corrected for the diffusion potentials arising from different ionic strengths within our sand tank using a commonly accepted model. Our experimental data can be reproduced by a simple model accounting for the effect of surface conductivity due to the electrical double layer coating the surface of the grains. Our results indicate that Hittorf transport numbers changing with salinity need to be considered when developing a holistic model. Furthermore, when considering the polarity and magnitude of the thermoelectric response, salinity and grain size are important factors.

iii

TABLE OF CONTENTS

LIST OF FIGURES

LIST OF TABLES

ACKNOWLEDGMENTS

I would like to express my gratitude to my adviser Dr. Andre Revil for all his support, suggestions, and expertise. I would also like to thank Dr. David Benson and Dr. Kamini Singha for all their help and support that made this possible.

In no particular order I would like to thank Dr. Pauline Kessouri, Justin Rittgers, Dr. Qifei Niu, Dr. Deqiang Mao, Paul ElKhoury, and Katie Radavich for their support and help throughout this project.

Finally I would like to thank my family for their continued support in all of my studies.

CHAPTER 1

INTRODUCTION

The self-potential method is a passive electrical geophysical method in which a measured electrical field (voltage) is used to characterize the distribution of electrical source currents within the subsurface of the Earth. In turn, this source current density can be related to the flow of pore water (streaming current, see Abaza and Clyde, 1969), the diffusion of ionic species (electrochemical diffusion potential or diffusion current, Ikard et al., 2012, Leinov and Jackson, 2014), the gradient of the redox potential in presence of a biotic or an abiotic electronic conductor (Risgaard-Petersen et al., 2012, Rittgers et al., 2013), and the thermoelectric current associated with a thermal gradient (Tasaka et al., 1965, Leinov et al., 2010, Leinov and Jackson, 2014).

1.1 Thermoelectric response in self-potential

The thermoelectric effect is the least understood and least studied contribution to self-potential signals. Several experiments have been published on the subject (Marshall and Madden, 1959, Nourbehecht, 1963, Corwin and Hoover, 1979), however, these data are unreliable because of their inability to account for temperature-related electrode effects. A phenomenological approach of the thermoelectric effect has been used recently to understand the self-potential signals associated with in situ coal seam fires (Revil et al., 2013, Karaoulis et al., 2014) and to develop some new techniques to localize preferential flow paths in the shallow subsurface via the injection of heated water (Ikard and Revil, 2014). The lack of reliable experimental data available on the thermoelectric effect make it difficult to test mechanistic models (Revil, 1999). Current models interpret the effect of temperature as an induced chemical potential with the movement of charge carriers (ions) and the heat of transport (Revil, 1999, Leinov and Jackson 2014, Tasaka et al., 1965).

An increasing thermal gradient is known to promote the permeation of ions through a porous material (Tasaka et al., 1965). Source currents associated with increasing temperature are known to be generated by the preferential mobility of ions in solution (Tasaka et al., 1965, Westermann-Clark and Christoforou, 1986). The preferential mobility of individual ions in a porous material increases the electrical conductivity of the affected pore water (Goodwin et al., 1899, Revil, 1999, Meyer and Revil, 2015).

There are two problems with most existing laboratory experiments on the thermoelectric effect. The first issue is that temperature can change the intrinsic potential of the electrodes, an effect that is difficult to account for (see an extensive discussion in Ikard and Revil, 2014). The simple solution for this problem is to avoid having the electrodes "contaminated" by temperature changes. The second issue with experimental data is the effect of temperature on the release of ions from the solid phase in the pore water solution or associated with preferential evaporation of the water in a warmer reservoir. This effect creates a higher ionic strength of the pore water on the side with the highest temperature. A concentration gradient associated with the temperature gradient generates a diffusion potential that is superimposed on the thermoelectric response. The potential generated in this way needs to be estimated and corrected from the raw self-potential measurements to obtain an intrinsic thermoelectric coupling coefficient.
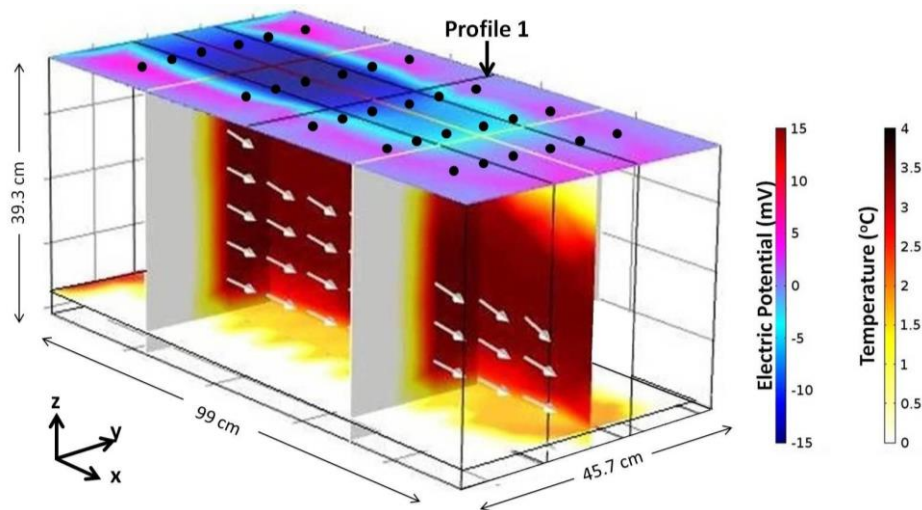
Figure 1.1 Simulation of self-potential generation by heated water advecting through a coarse grain channel in the subsurface. The anomaly of self-potential is shown on the top down profile, and the heat signature is shown with crossed 2-D panels. Modified from Ikard and Revil 2014.

1.2 Research motivations

The motivation for this work follows the work of Ikard and Revil (2014), where self-potential was used to passively detect an advecting warm water pulse through a preferential flow path (Figure 1.1). The experiment successfully showed that a change in water temperature can be detected by self-potential responses in a shallow aquifer. A thermoelectric coupling coefficient

(C_T) was difficult to determine with the data obtained because the electrodes themselves were affected by the temperature increase of the advecting water. The temperature effect on the Ag/AgCl non-polarizing electrodes that were used is relatively large in comparison to the thermoelectric response. This uncertainty in the thermoelectric response prompted the desire to better understand the C_T in unconsolidated sands.

1.3 Research objectives

This research aims to test the current principals that govern the thermoelectric response. If a viable theory could be demonstrated, a heat tracer could be used in place of a saline tracer to detect preferential flow paths in an earthen embankment as in Ikard et al. (2012), providing a more quantitative assessment water passing through a preferential flow path within earthen embankments and levees without salt contamination of the water in interest.

In this study, a simple approach is developed to estimate the thermoelectric coupling coefficient while avoiding the electrode effect and correcting for the diffusion potential. We will begin to establish database of experimental data for clean silica sands at various salinities. The measurement of the intrinsic thermoelectric coupling coefficient will be compared to a mechanistic model. The intent is that this database will be used in turn to gain a better understanding of the fundamental mechanisms controlling the thermoelectric coupling in porous media.

CHAPTER 2

THERMOELECTRIC THEORY

A common language discussion of the theory behind the source current of the thermoelectric coupling phenomena is necessary before physics is used. There are inconsistencies in literature as to how the self-potential signals are generated and the application of the mathematics, such as the polarity of the generated potential. This basic discussion will help show how and why it is important to be consistent here.

First, source currents generated by a diffusion potential in a NaCl electrolyte occur when there is a solute concentration gradient present. The mechanism that generates an electric potential is the relative mobility of ions through a given media. In this case sodium (Na^+) ions are known to travel slower than the co-ion, chloride (Cl^-) (Valkenburg et al., 2005, Jougnot et al., 2015). The hydrated radius of Na^+ is larger than that of Cl^-, decreasing its relative mobility within the pore water (Nightingale, 1959, Jougnot et al., 2015).

Diffusion of ions occurs due to random Brownian motion. The frequency of ion collision is greater where there is a greater amount of solute in a solution. This causes a natural tendency for ions to migrate towards a lower concentration (Figure 2.1a). The Hittorf number determines the relative rate at which the diffusion occurs (Jougnot et al., 2015). This disproportional rate of diffusion causes negative charge to build on the low concentration side and a relative positive charge in the high concentration side that migrates slower. If one were to measure the voltage with a reference electrode on the high concentration side, the polarity would be negative and when the electrodes were swapped an equal magnitude but opposite polarity would be observed. This phenomena is known as diffusion potential (Revil, 1999, Leinov and Jackson 2015, Figure 2.1a).

When considering the self-potential generated beginning with a homogeneous concentration but differentially heated system the source current occurs the same way as the diffusion potential (Figure 2.1b). The ions in a NaCl solution are considered "thermophobic" (Vigolo et al., 2010), meaning that solute travels away from a heat source. A warmer solution has more energy causing more random collisions when compared to a colder area (Figure 2.1a). Therefore the ions naturally migrate from high temperature to low temperature. The same differential mobility principals cause a separation of charge as discussed before. Again considering

4

a) Concentration-driven diffusion

Low salinity
(low collision rate)

High salinity
(high collision rate)

b) Temperature-driven diffusion

Low temperature
(low collision rate)

High temperature
(high collision rate)
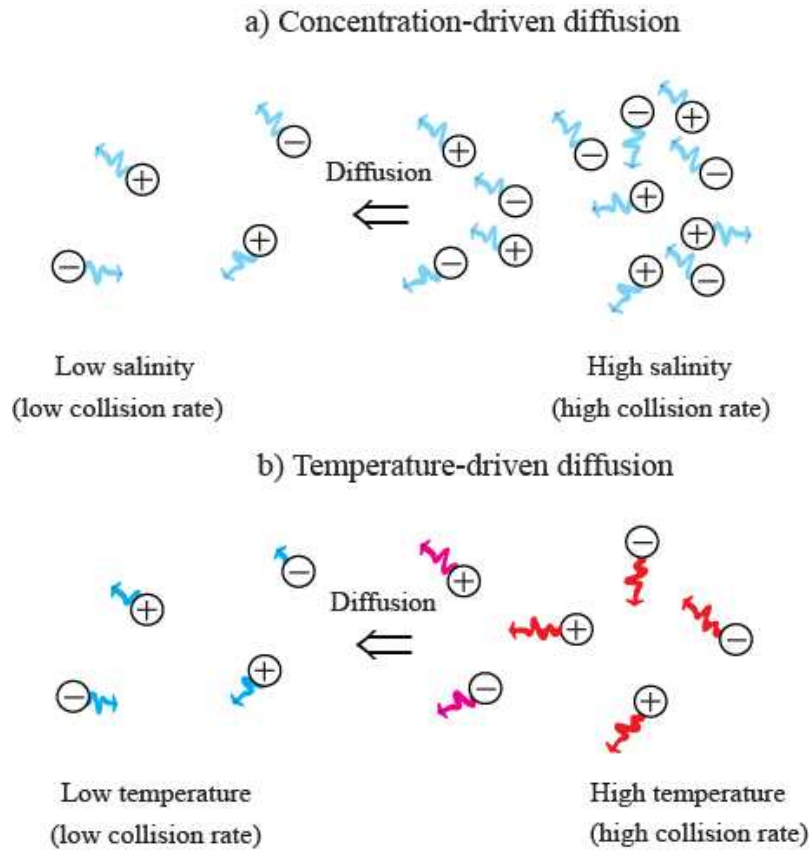
Figure 2.1 Diffusion of a 1:1 electrolyte. Diffusion of ions induced by a concentration gradient related (a) and a temperature driven diffusion of ions, in a thermophobic ionic solution (b) are shown to diffuse away from locations of high concentration and high temperature. The amount of ion collisions in a given area determine the direction of ion diffusion. In high concentration areas the amount of ion collisions is greater than in low concentration. In high temperature areas thermal agitation causes the migration of ions. Figure taken from Meyer and Revil (2015).

a measurement with a reference electrode on the warm side of the tank, one would expect the polarity to be negative. The thermoelectric coupling coefficient (C_T), which is defined as the ratio of change in potential over the change in temperature $\left(\dfrac{\Delta \psi}{\Delta T}\right)$, would be considered negative as well.

Now considering a porous material with a charged mineral surface, such as silica sands. The charging of the mineral surface is usually from amphoteric reactions between the mineral surface and the pore water, (Revil, 1999, Revil and Skold, 2011). To understand the source current
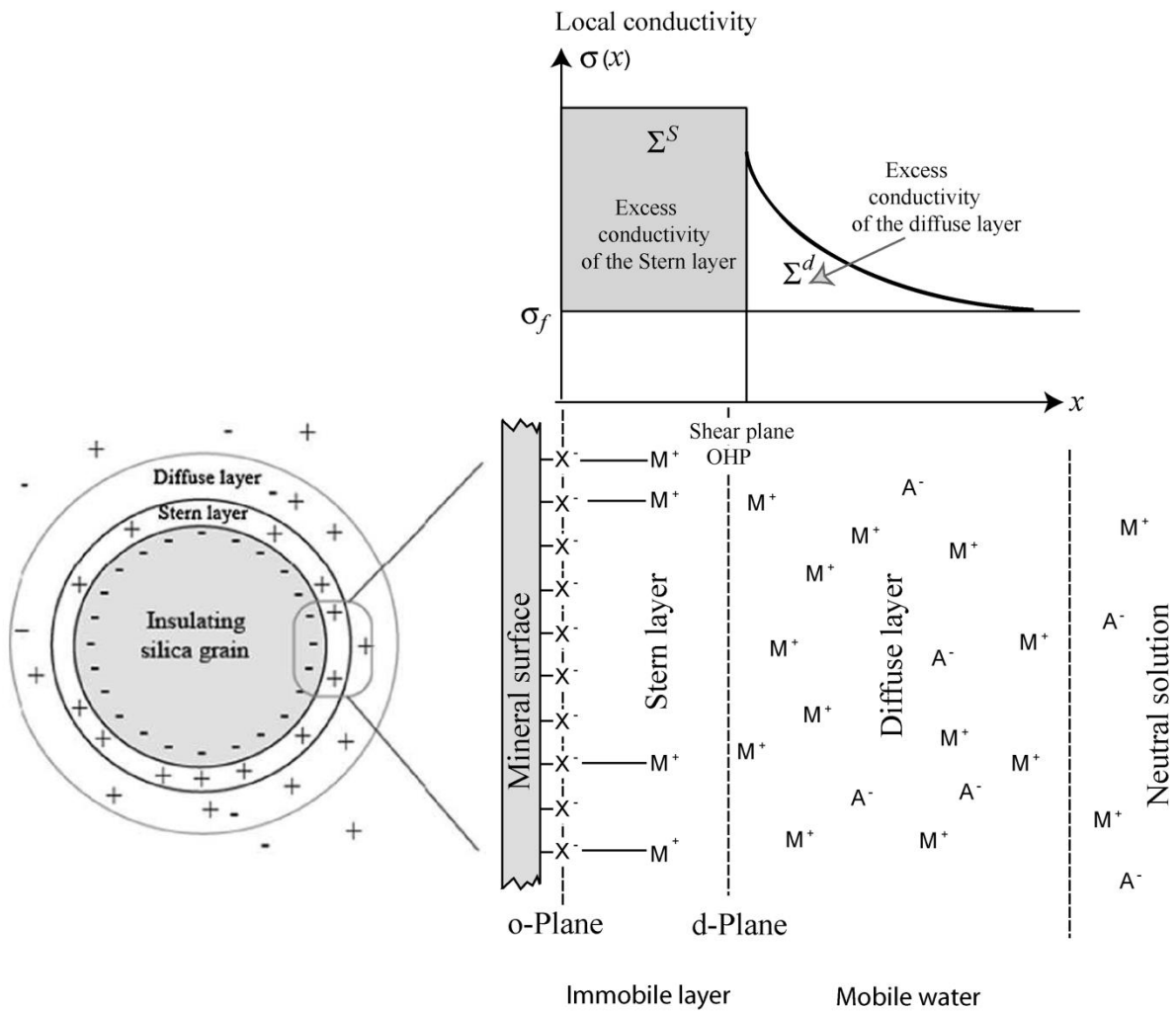
Figure 2.2 Electrical double layer conceptual model. The negative mineral surface charges are counter balanced by immobilized positive ions in the Stern layer and mobile positive ions in the diffuse layer. The shear plane (d-plane) identifies the surface where the relative velocity of the solid phase with respect to the fluid phase is zero. The electrical conductivity with respect to the distance away from the grain surface is the sum of the pore fluid conductivity (σ_f) with the excess surface conductivity (Σ^S) in the Stern layer. Adapted from Revil et al. (2014) and Revil and Mahardika (2013).

associated with most self-potential measurements, an understanding of the electrical double layer in porous media is required. When a porous material is saturated with an electrolyte solution interactions occur between the ions in solution and the material surface (Revil and Mahardika,

2013). In the case of a silica grain the charge of the surface (σ_s) is negative. The surface of the grain becomes surrounded by co-ions, in this case, cations. This layer that immediately surrounds the grain is called the Stern layer (Stern, 1924). The Stern is known to immobilize the coion in solution and is net positive in charge. The immediate layer surrounding the Stern layer is known as the diffuse layer (Figure 2.2). The Stern layer and the diffuse layer make up the electrical double layer surrounding a silica grain. The diffuse layer is the layer of ions that is mobile, and has a net charge similar to that of the Stern layer (Figure 2.2). Adsorption occurs within the Stern layer, this charge is considered fixed in place (Figure 2.2). In the case of silica, the grain surface is negatively charged and the pore water has a slight excess of positive charge from the diffuse layer countering the silica grain's negative charge (Figure 2.2).

There are two extreme end-member cases that must be considered here. At high salinity the pore water can be considered electroneutral, there is no effect from the small amount of excess positive charge in the diffuse layer (Figure 2.2). This case is the same as discussed above where the differences in Hittorf ion transport reflect the source potential, with a tortuosity correction taken into account in a porous material. The expected thermoelectric response stays negative in this case. At very low salinities the diffuse layer's net positive charge has a significant effect on the nature of the thermoelectric response. In this case the Hittorf number (T_+) for the positive ion reaches unity, see discussion in Chapter 3 (also see Revil and Jougnot, 2008). This means that in effect all the current is carried by the positive ions at very low salinities. The thermoelectric effect would be positive in this case where positive ions are diffusing from high to low temperature.

2.1 The thermoelectric effect

The physical relationships of thermoelectric response within the experimental design are reviewed here. A saturated porous material with a binary symmetric 1:1 electrolyte such as NaCl is considered. In the absence of pore water flow, Equation 1 shows the coupled constitutive relationship derived by Revil (1999),

$$\begin{bmatrix} \mathbf{J}_{(+)} \\ \mathbf{J}_{(-)} \\ \mathbf{J}_s \end{bmatrix} \simeq - \begin{bmatrix} \dfrac{\sigma_{(+)}}{e^2} & 0 & \dfrac{1}{T}\dfrac{\sigma_{(+)}}{e^2}Q_{(+)} \\ 0 & \dfrac{\sigma_{(-)}}{e^2} & \dfrac{1}{T}\dfrac{\sigma_{(-)}}{e^2}Q_{(-)} \\ \dfrac{1}{T}\dfrac{\sigma_{(+)}}{e^2}Q_{(+)} & \dfrac{1}{T}\dfrac{\sigma_{(-)}}{e^2}Q_{(-)} & \dfrac{\lambda}{T} \end{bmatrix} \begin{bmatrix} \nabla\tilde{\mu}_{(+)} \\ \nabla\tilde{\mu}_{(-)} \\ \nabla T \end{bmatrix}, \quad (1)$$

where $\mathbf{J}_{(\pm)}$ denote the fluxes of the cations (+) and anions (-), $\mathbf{J}_S$ is the flux of entropy (source current density generated by heat being transmitted by the physical movement of ions), T denotes the absolute temperature (K), $\sigma_{(\pm)}$ denotes the contribution to the electrical conductivity of the porous material (i.e., $\sigma_{(\pm)} = \sigma_{(+)} + \sigma_{(-)}$), e denotes the elementary charge (1.6×10^{-19} C), $Q_{(\pm)}$ is called the standard single-ion heat of transport (it represents the heat transported along with a unit diffusion flux of cations and anions, see Agar et al., 1989), λ denotes the thermal conductivity of the material (W m^{-1}K^{-1}), and $\tilde{\mu}_{(\pm)}$ denotes the electrochemical potentials of the cations and anions. See Table 2.1 for values used throughout this study. In non-isothermal conditions, the gradient of these electrochemical potentials are given by (e.g., Leinov et al., 2010),

$$\nabla\tilde{\mu}_{(\pm)} = k_b T \nabla \ln C_{(\pm)} - (\pm e)\mathbf{E} - S_{(\pm)}\nabla T , \qquad (2)$$

or alternatively,

$$\nabla\tilde{\mu}_{(\pm)} = k_b T \nabla \ln C_{(\pm)} - (\pm e)\mathbf{E} - (s_{(\pm)}^0 - k_b \ln C_{(\pm)})\nabla T , \qquad (3)$$

where k_b = 1.381×10^{-23} J K^{-1} denotes the Boltzmann constant, $C_{(\pm)}$ mV C^{-1} denotes the concentration of the cations and anions (equal to the salinity C_f in the two reservoirs in contact with the end-faces of the core sample, see experimental section in Chapter 4), $\mathbf{E}$ (V m^{-1}) denotes an externally applied electrical field (within the quasistatic limits of the Maxwell equations, it is found that $\nabla \times \mathbf{E} = 0 \Rightarrow \mathbf{E} = -\nabla\psi$ where ψ (V) denotes the electrical potential), and $S_{(\pm)}$ denote the partial entropies of the ions in the pore water while $s_{(\pm)}^0$ denotes the partial entropies of the ions in the pore water at a given salinity (then $S_{(\pm)} = s_{(\pm)}^0 - k_b \ln C_{(\pm)}$).

The total current density $\mathbf{J}$ (in A m^{-2}) can be written as,

$$\mathbf{J} = e(\mathbf{J}_{(+)} - \mathbf{J}_{(-)}) , \qquad (4)$$

After few algebraic manipulations and using the definitions of the macroscopic Hittorf numbers (dimensionless) it is found that,

$$T_{(\pm)} = \frac{\sigma_{(\pm)}}{\sigma} , \qquad (5)$$

(with the property $T_{(+)} + T_{(-)} = 1$) equation 6 is obtained,

$$\mathbf{J} = -\sigma\nabla\psi - \frac{k_b T}{e}\sigma\left(2T_{(+)}-1\right)\nabla\ln C_f - \frac{\sigma}{e}\left[T_{(+)}\left(\frac{Q_{(+)}}{T}-S_{(+)}\right)-(1-T_{(+)})\left(\frac{Q_{(-)}}{T}-S_{(-)}\right)\right]\nabla T. \quad (6)$$

The first term of equation (6) corresponds to Ohm's law, the second term to the diffusion current, and the third term to the thermoelectric current. The total current density in a porous material can be described by a constitutive equation taking the form of a generalized Ohm's law for the total current density $\mathbf{J}$ (A m^{-2}),

$$\mathbf{J} = \sigma\mathbf{E} + \mathbf{J}_S, \quad (7)$$

where, σ denotes the bulk electrical conductivity of the porous material (S m^{-1}), and $\mathbf{J}_S$ (A m^{-2}) denotes any internal source current density.

Table 2.1 Summary of parameter values used in all equations (Lide, 2009, Agar et al., 1989).

Parameter	Units	Value
k_B	J K^{-1}	1.3806504×10^{-23}
e	C	$1.602176487\times10^{-19}$
t_+	-	0.3962
Q_+^*	J mol^{-1}	3460
Q_-^*	J mol^{-1}	530
s_+^0	J mol^{-1} K^{-1}	59.0
s_-^0	J mol^{-1} K^{-1}	56.5
N_A	mol^{-1}	6.02214179×10^{23}
T	K	298.15

According to equations 6 and 7, the occurrence of an electrical potential is driven by the existence of a temperature gradient and a salinity gradient. It was found that during the experimental process a salinity gradient not due to the temperature-induced permeation of ions began to develop. This effect, known as the diffusion potential, is superimposed on the thermoelectric response. During an experiment, a salinity gradient can arise because of the dissolution of some minerals associated with the sand or, the evaporation of the water in one of the reservoir.

The thermoelectric coupling coefficient is defined as,

$$C_T = \left(\frac{\partial \psi}{\partial T} \right)_{\mathbf{J}=0}. \tag{8}$$

This coefficient is usually expressed in mV °C^{-1} for convenience (V K^{-1} in SI units). This coefficient is usually the one that is experimentally derived and given in the literature. However, if salinity gradients have been generated during the experiment, they need to be taken into account. Equations (6) and (7) are used to define an apparent thermoelectric coupling coefficient once the salinity effect has been corrected for. Rearranged here the thermoelectric coupling coefficient is defined as,

$$C_T = \frac{1}{e} \left[T_{(+)} \left(S_{(+)} - \frac{Q_{(+)}}{T} \right) - (1 - T_{(+)}) \left(S_{(-)} - \frac{Q_{(-)}}{T} \right) \right]. \tag{9}$$

In addition, the partial entropies are related to the concentrations according to: $S_{(\pm)} = s_{(\pm)}^0 - k_b \ln C_{(\pm)}$, therefore,

$$C_T = \frac{1}{e} \left[T_{(+)} \left(s_{(+)}^0 - \frac{Q_{(+)}}{T} \right) - (1 - T_{(+)}) \left(s_{(-)}^0 - \frac{Q_{(-)}}{T} \right) \right] - \frac{k_b}{e} (2T_{(+)} - 1) \ln C_f. \tag{10}$$

2.1.1 The microscopic and macroscopic Hittorf transport number

The Hittorf method has been used to determine ions relative mobility within a given solution (Goodwin et al., 1899, Levy, 1952, Revil, 1999, Leinov and Jackson, 2014, Jougnot et al., 2015). It is commonly determined in laboratory measurements by measuring the concentration of electrolyte in the anode and cathode compartments of a sealed system after the induction of current for a set period of time (Levy, 1952, Negi and Anand, 1985).

The relative mobility of an individual ion can be expressed by the microscopic Hittorf number (t_{ion}) and is defined as the ion mobility (β_{ion}) divided by the sum of all ions mobility in solution, $t_{ion} = \frac{\beta_{ion}}{\sum_{i=1}^{n} \beta_{ion}}$ (Jougnot et al., 2015), or in a NaCl solution $t_{Na} = \frac{\beta_{Na}}{\beta_{Na} + \beta_{Cl}}$ and

$t_{Cl} = \frac{\beta_{Cl}}{\beta_{Na} + \beta_{Cl}}$ where, $t_{Na} + t_{Cl} = 1$. Accepted literature values for the microscopic Hittorf numbers are approximately 0.39 and 0.61 for Na$^+$ and Cl$^-$ respectively for the binary NaCl electrolyte (Leinov and Jackson, 2014, Gulamali et al., 2011. When moving to a larger scale (macroscopic)

10

within a porous media, factors such as the surface conductivity (σ_s), and the formation factor (F) within a given media must be taken into account to determine an accurate Hittorf transport number.

Equation 10 shows that the coupling coefficient depends heavily on the value of the macroscopic Hittorf number $(T_{(\pm)})$ of the porous material. An expression for this Hittorf number for clean sands is needed to properly characterize the system. Revil and Skold (2011) studied the complex conductivity of sands including the effect of surface conductivity, which is non-zero even in clean sands (see recently Revil et al., 2014 for the Fontainebleau sandstone). The expression they obtain for the conductivity (see their equation 4) is,

$$\sigma = \frac{1}{F}\sigma_w + \frac{F-1}{F}\sigma_S .$$ (11)

where σ_w and σ_S denotes the conductivity of the pore water and the surface conductivity coating the surface of the grains, respectively, and F is the intrinsic formation factor. Using Archie's first law (Archie, 1942, Revil et al., 1998) $F = \phi^{-m}$ where, ϕ is the porosity of the sand, and m is the cementation factor. For a sand with a narrow grain size distribution, the surface conductivity can be written as,

$$\sigma_S = \frac{4}{d_{50}}\Sigma^S .$$ (12)

Where d_{50} denotes the median grain size and Σ^S denotes the specific surface conductance of the electrical double layer (typically $\Sigma^S = 4\times10^{-9}$ S). In the case of broad grain size distribution, Revil and Florsch (2010), provides a way to compute the surface conductivity as a function of the particle size distribution. See Table 2.2 for properties of the sands used.

Since this surface conductivity is associated with mostly a cationic contribution,

$$\sigma_{(+)} = \frac{1}{F}t_{(+)}\sigma_w + \frac{F-1}{F}\sigma_S ,$$ (13)

$$\sigma_{(-)} = \frac{1}{F}t_{(-)}\sigma_w ,$$ (14)

where $t_{(\pm)}$ denotes the microscopic Hittorf numbers of the cations and anions in the pore water. When considering a NaCl solution, $t_{(+)} \approx 0.39$ independent of the temperature. Therefore, the macroscopic Hittorf number is given by,

11

$$T_{(+)} = \frac{t_{(+)}\sigma_w + (F-1)\dfrac{4}{d_{50}}\Sigma^S}{\sigma_w + (F-1)\dfrac{4}{d_{50}}\Sigma^S}.\tag{15}$$

At high salinity, it is easy to see that surface conductivity would be much smaller than the bulk pore water conductivity and therefore $T_{(+)} = t_{(+)}$. At low salinity, surface conductivity can dominate and $T_{(+)} \approx t_{(+)}$. It follows that the intrinsic coupling coefficient can reach the following bounds (now using molar quantities),

$$C_T = \frac{1}{eN_A}\left[t_{(+)}\left(s_{(+)}^0 - \frac{Q_{(+)}}{T} \right) - (1-t_{(+)})\left(s_{(-)}^0 - \frac{Q_{(-)}}{T} \right) \right] - \frac{k_b}{e}(2t_{(+)} - 1)\ln C_f,\tag{16}$$

$$C_T = \frac{1}{eN_A}\left(s_{(+)}^0 - \frac{Q_{(+)}}{T} \right) - \frac{k_b}{e}\ln C_f.\tag{17}$$

At high and low salinities, respectively, and where N_A denotes Avogadro's number (6.02×10^{23}). Lide (2009) and Agar et al. (1989, Table 2.1) provides some values for the parameters entering the previous equations. Considering a NaCl solution, $t_{(+)} \approx 0.39$, $Q_{(+)}$ = 3460 J Mol^{-1}, $Q_{(-)}$ = 530 J Mol^{-1}, $s_{(+)}^0$ = 59.0 J Mol^{-1} K^{-1}, $s_{(-)}^0$ = 56.5 J Mol^{-1} K^{-1}, and using T = 298.15 K (Table 2.1). Note that eN_A denotes the Faraday's constant (96,320 C Mol^{-1}) for the salinity independent term existing in equations 16 and 17, this yields a low salinity bound of C_T = + 0.5 mV K^{-1} while at high salinity -0.2 mV K^{-1} (see Figure 3.1).

Table 2.2 Silica sand properties used in T_{Na} calculations (some values taken from Sakaki, 2009), others taken as estimates from similar high silica sands.

Sand Properties	Unimin Corp. 4095	Unimin Corp. 7030
Porosity (ϕ) [-]	0.411	0.418
Cementation exponent (m) [m^{-1}]	1.3	1.3
Specific Surface Conductivity (Σ^S) [S m^{-1}]	4×10^{-9}	4×10^{-9}
Median Grain Size (d_{50}) [mm]	0.72	0.2
Formation Factor (F) [-]	3.18	3.11
Surface Conductivity (σ_s) [S m^{-1}]	1.52×10^{-5}	5.43×10^{-5}

CHAPTER 3

THERMOELECTRIC MODELING

Models for the thermoelectric coupling coefficient have been presented by several authors for porous media in a simple electrolyte solution (Tasaka et al., 1965, Revil, 1999, Leinov and Jackson, 2014). Each is based on diffusion kinetics of the corresponding ions, see Equations 16 and 17.

Here, the mechanistic model end-members described in chapter 2 are first used to bind the theoretical range of the thermoelectric coupling coefficient through four orders of magnitude in salinity (Figure 3.1). The end-members are generated from using two separate, constant macroscopic Hittorf numbers ($T_{Na} = 0.3962$, and $T_{Na} = 1$). Next, the model is then adapted to develop a relationship between sand properties and the macroscopic Hittorf number to easily and more accurately predict the thermocouple coefficient from high to low salinities.

3.1 Modeling the theoretical thermocoupling coefficient

The models we begin with are identical to models presented by Leinov and Jackson (2014). Equation 18 is equivalent to Equation 16 for a NaCl solution. The concentrations are changed to activities of the solution through,

$$C_T = \frac{\Delta \psi}{\Delta T} = -(2T_{Na} - 1)\frac{k_b}{e}\ln(a) + \frac{1}{N_A}\left[\frac{T_{Na}}{e}\left(s_{Na}^0 + \frac{Q_{Na}^*}{T}\right) - \frac{T_{Cl}}{e}\left(s_{Cl}^0 + \frac{Q_{Cl}^*}{T}\right)\right], \tag{18}$$

and,

$$T_{Na} + T_{Cl} = 1, \tag{19}$$

where a is the activity of the solution, N_A is Avogadro's number, s_{Na}^0 and s_{Cl}^0 are the molal entropies for sodium and chloride ions respectively (Lide, 2009), and Q_{Na}^* and Q_{Cl}^* are the representative cross-coupling coefficients between the temperature gradient and salinity gradient, respectively (Agar et al., 1989) (Table 2.1). For the study presented here, it is assumed that the ratio of $\frac{Q_{Na,Cl}^*}{T}$ is constant, and that the temperature (T) corresponds to the reference temperature discussed in Agar et al. (1989) (see Table 2.1). The validity of this assumption is beyond the scope
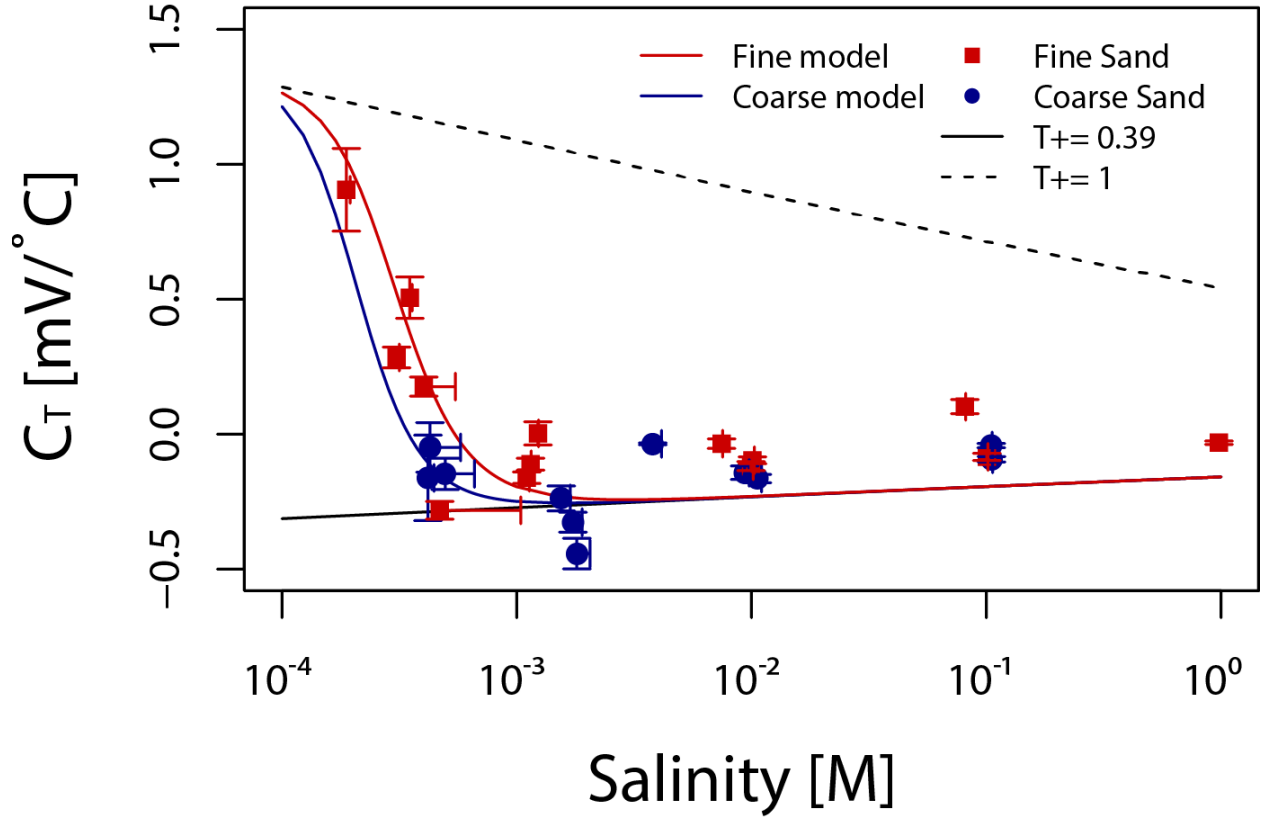
Figure 3.1 Measured thermoelectric response (mV/C) over four orders of magnitude salinity (M). Red squares indicate the fine (7030) type sand, blue circles indicate the course (4095) sand. Adapted model curves are generated with a calculated surface conductivity (σ_s) and formation factor (F) using Equation 18. The solid black theoretical C_T bounding line is generated through Equaiton 18 where $T_{NA/+} = 0.3962$. The dotted black line represents Equation 21 where $T_{NA/+} = 1$. The error in experimental measurenets is reported as residual standard error. Data presented here are discussed in Chapter 4 and Appenix A and B.

of this study and has been found to be a reasonable assumption to make (Leinov and Jackson, 2014).

As discussed in Chapter 2, there are two end-members represented in equation 18. One where the macroscopic Hittorf transport number for sodium (T_{Na}) is equivalent to the microscopic Hittorf transport number,

$$T_{Na} = t_{Na} = 0.3962. \tag{20}$$

This assumption is valid up to 0.09 M but only increases by 2.5% for salinities above 0.09 M in this study where our maximum salinities are approximately 1 M (Leinov and Jackson, 2014, Gulamali et al., 2011). Hence, for this study $t_{Na} = 0.3962$ is used throughout.

The other end-member where $T_{Na} = 1$ is presented in Equation 16 in this case can be represented as,

$$C_T = \frac{\Delta \psi}{\Delta T} = -\frac{k_B}{e} \ln(a) + \frac{1}{N_A e} \left(s_{Na}^0 + \frac{Q_{Na}^*}{T} \right).$$ (21)

Equations 18 and 21 are represented in Figure 3.1 by the straight lines that bound the theoretical response.

A model is created for each grain size tested here (Figure 3.1). The model shows how the C_T for each grain size would change across the range of salinities tested. Assuming that only T_{Na} in Equation 18 is changing throughout the set of experiments, forward modeling is performed by inputting a range of salinities into Equations 14-16 to determine a hypothetical T_{Na}. This range of hypothetical T_{Na} is then input into Equation 18 for each grain size (Figure 3.1), generating a C_T at a given salinity (fine and course models, Figure 3.1).

3.2 Summary of model results

The end-members of C_T are easily defined by the theory in Chapter 2 and mostly encompass the data collected herein (Figure 3.1). Predictions of C_T are found to be much more accurate when the physical characteristics of the media can be estimated. These physical characteristics can be used to determine $T_{NA/+}$ for a given pore water conductivity (σ_w), surface conductivity (σ_s) and grain diameter (d_{50}). The $T_{NA/+}$ can then be used in the known theory to more closely determine a C_T for a given salinity.

CHAPTER 4

TANK EXPERIMENT

Here, a method is developed to help experimentally determine C_T over a range of salinities. The experimental design is outlined, then data acquisition is discussed in detail. Finally, Data interpretations and corrections are discussed. This method attempts to isolate the self-potential thermoelectric response but it is found that a diffusion potential response must be taken into account and removed from raw data to isolate the thermoelectric response.

4.1 Experimental setup

The tank used for this study was constructed out of 0.635 cm thick acrylic. Dividers were constructed at 6 cm from either end, using 160 thread/inch polyester mesh attached to an acrylic frame to form a permeable barrier between each side of the tank and the sand chamber (Figure 4.1). The tank dimensions are 11.7 cm deep, 32.4 cm long, and 12.2 cm wide. The volume of the tank is approximately 4.6 L.

Before each experiment, saline water was prepared at least one day prior, and sat in the same room over night or longer to equilibrate to the room temperature. Prior to each test, all sand material was first triple rinsed with deionized (DI) water in order to remove any particulates or salt that may have originated from the manufacturer (Sakaki, 2009). Prior to each experiment the DI-rinsed sand was also thoroughly rinsed with the prepared saline water that was to be used. A wet pack was performed on the day of each experiment, the saline water was first poured into the tank, and the pre-rinsed sand was then added in small amounts and stirred to have a uniform/homogeneous sand pack. This method also ensures that there are limited air bubbles in pore space between sand grains. Sand was added until there were two centimeters left from the top of the tank. One centimeter of water was then removed from the top of the sand so that the electrodes would not be sitting in water when taking measurements while maintaining saturation. Each experiment used about 4.1 kg of sand and 2.5 L of saline water. The cold and hot sides of the tank are separated by the sand in-between (Figure 4.1). The cold water reservoir was either filled with ice water or kept at room temperature depending on the type of experiment performed.

There were high temperature gradient (HTG) and a low temperature gradient (LTG) regimes tested. In the HTG some salt was added to reduce the temperature close to or below 0°C

in the cold reservoir. A Johnson A419 temperature control device (Johnson Controls 2015) was used in conjunction with a heating element in the hot reservoir. A vinyl tube was attached to a small submersible water pump placed in each reservoir. Each tube was looped into the corresponding side of the tank and then looped back into the reservoir (Figure 4.1). To reiterate, the reservoirs that are being heated or cooled are not in hydrologic connection with the tank. The heat energy is transferred from the reservoir to the sides of the tank through vinyl tubing (Figure 4.1). This method allowed for heating and cooling the room temperature tank water without disturbing the desired hydrostatic nature of the sand tank. This method also allows the salinity in the tank to be isolated from the reservoir salinity. Petiau (Pb/PbCl) non-polarizing electrodes were used (Petiau, 2000) with an AMEC MX 55 (resolution ±0.01 mV) multimeter to measure the self-potential field. Temperature was measured using an FI 308 (0.3% measurement ±1 digit) from Française d'Instrumentation with a K type (chromel-alumel) thermocouple. Salinity was measured with an Orion Versa Star Conductivity meter (0.5% of reading ±1 digit).
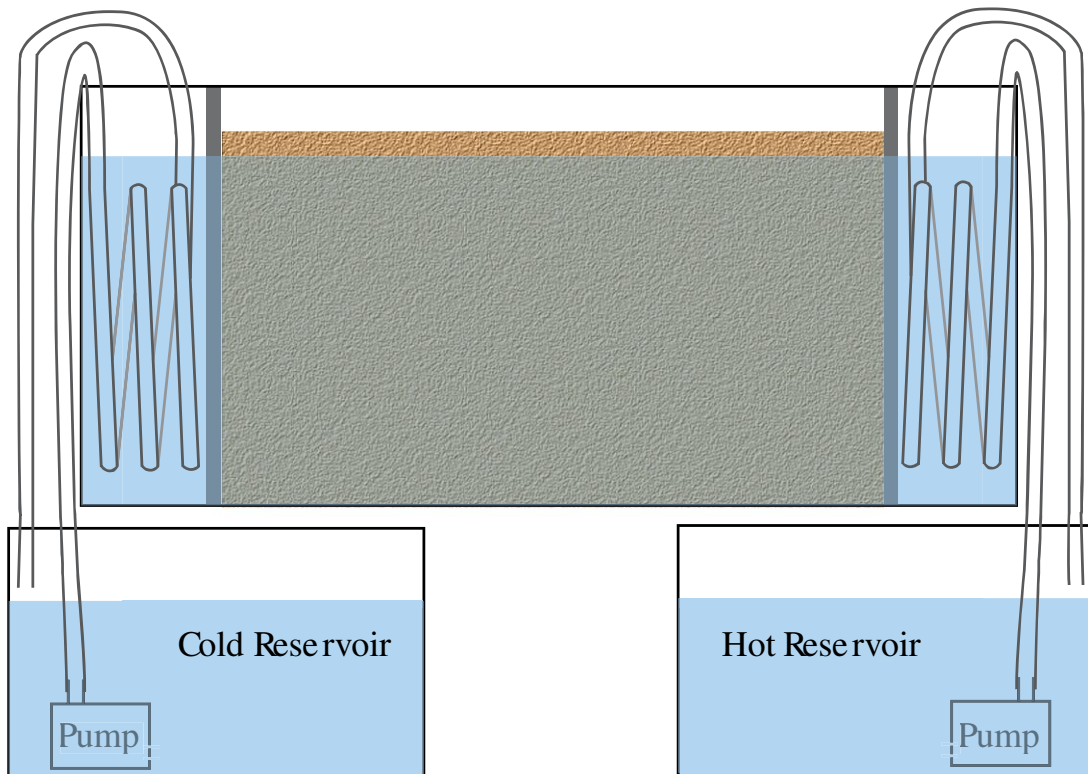
Figure 4.1 Side view schematic of tank and reservoir setup. Hydrosatic head is maintained througout the experiment and heat is transferred into the tank by the vinyl chloride tubes as shown. Sand is shown in the center and held there by permeable mesh dividers in grey.
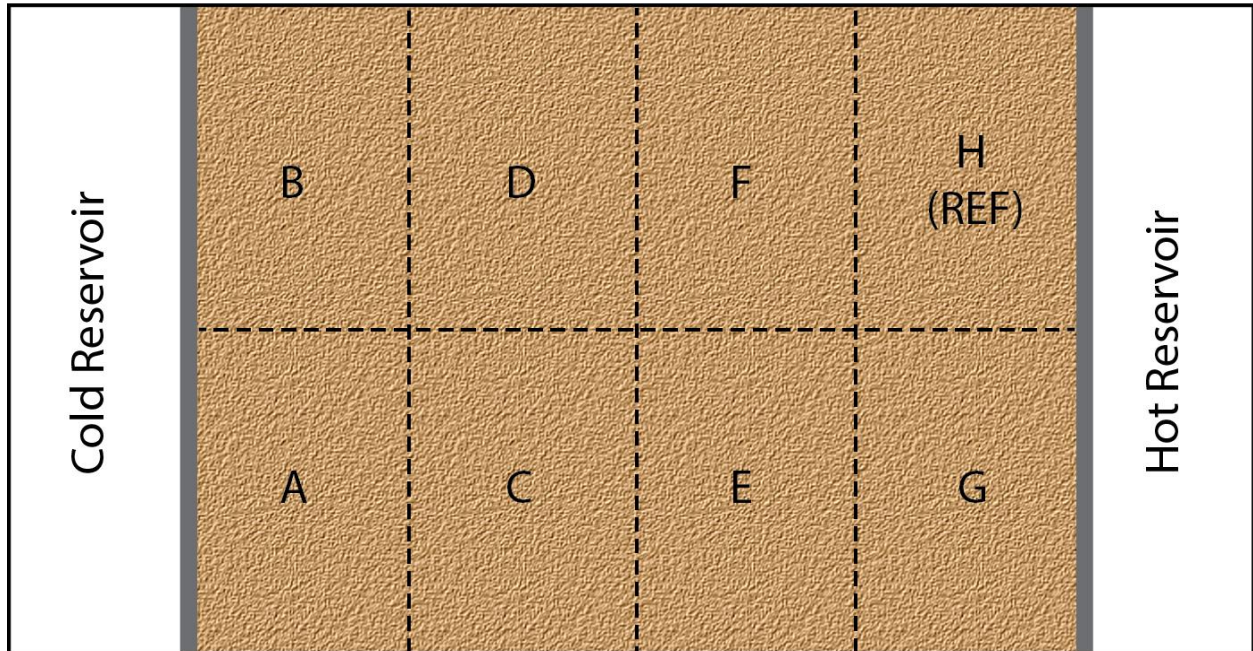
Figure 4.2 Top view schematic of tank including sampling locations and location of the reference electrode. Each sampling location is equally spaced and measurements were made in the center of the space.

4.1.1 Data acquisition

A total of 25 experiments were conducted to determine the effects of various salinities and temperature regimes on the measured thermoelectric coupling coefficient C_T. A total of 11 experiments were performed for the #4095 sand and 14 experiments were performed with the #7030 sand. For the complete data set see Appendices A and B.

The HTG regime of experiments kept the cold reservoir at 0°C ± 5°C and the hot reservoir was increased from room temperature to 90°C ± 5°C over the course of the experiment. The LTG regime kept the cold reservoir at room temperature (~20°C) and the hot water reservoir is increased to 35°C ± 2°C. There is no distinction made between HTG and LTG experiments in the final C_T data presented. It should be noted that the HTG showed greater variation in salinities and standard errors of measured potential in comparison to the LTG experiments in all salinities tested. All data appear to follow a similar trend regardless of the temperature regime tested. This being said, a lower temperature regime was eventually preferred because of the wear on equipment.

Each experiment started with the tank water and sand at room temperature, which was typically 20°C± 4°C. This was accomplished by storing the sand and saline water in the same room

that the experiment was done for some time prior to commencement data collection. The tank was divided into 8 equally spaced sampling locations (Figure 4.2). Initial condition measurements were taken every ten minutes for sixty minutes or more before each experiment began. Pumps in each of the reservoirs were run throughout the initial condition measurements and data collection in each experiment in order to remove any spurious potentials that may be generated by the pumps. The purpose of collecting the initial condition data was to measure any average background potential that may have existed across the tank prior to each experiment, so these steady-state values could be removed from the potentials of interest that are induced when the tank temperature was changed. For each measurement set, the temperature and electric potential are measured in the center of each of the 8 locations in the tank. The temperature data were recorded first and immediately after self-potential measurements were recorded. Self-potential data were recorded using the same reference electrode that was always placed in the same location (Figure 4.2). Salinity measurements were made in the hot and cold sides of the tank for each sample during the experiment as well. A total of seven potential measurements were taken every sampling period using a short-duration contact with the sand surface at locations A-G (Figure 4.2). Just before and directly after the seven potential measurements are made, a tip-to-tip voltage is taken. The tip-to-tip voltage shows the drift of the electrodes over the sampling period. A tip-to-tip voltage is a ground or reference to which all measurements can be referenced from. Essentially setting each measurement to a common zero potential to be referenced from. This sequence and method of sampling keeps the thermocouple wire separate from the electrodes, eliminating possible interference. This method also limits the amount of time that each electrode can be influenced by the temperature of the sand, minimizing electrode drift due to temperature throughout the experiment.

Initial condition measurements are completed over the course of an hour or more before each experiment, where the temperature in the tank is uniform (± 0.4°C) at room temperature, a constant hydrostatic head, and a constant salinity (±< 10%) is maintained throughout the tank. Depending on the temperature gradient tested, the heater was turned on to 90°C (HTG) or 35°C (LTG). The cold water reservoir was left at room temperature (LTG) or decreased with ice to near zero centigrade (HTG). It is important to note that the tank temperature does not reach the same temperature as the water reservoirs during the course of the experiment, due to thermodynamic

limitations imposed by the finite thermal conductivities of the apparatus and materials used, as well as heat transfer with the surrounding environment.

Ten minute sampling intervals were employed for the initial condition measurements. The sampling intervals used after the initial condition measurements were either a ten or thirty minute time period. A ten minute sampling interval was typically used at the beginning of an experiment, and then adjusted to a thirty minute sampling interval as the temperature gradient across the tank approached equilibrium. Each experiment lasted anywhere between 4 to 6 hours.

4.1.2 Data interpretation

Initial review of the C_T with measurements taken from locations A-G (Figure 4.2) referenced from location H lead to a data set that did not corroborate with models and theory. The intention of measuring all these locations across the tank was to get a sense of how the C_T was changing throughout the experiment, a snapshot of C_T every time a measurement was made. It was found that the method we were using to correct for salinity (diffusion potential) could not be applied to measurement locations other than A and B (Figure 4.2). The diffusion potential corrections use a salinity measurement made in the open water on each side of the tank (Figure 4.1) and could not be applied to measurements C-G. The only locations where the diffusion potential corrections were found to be valid were locations A and B, which were in closest proximity to the salinity measurements themselves. Therefore, the method found to best determine the thermocoupling coefficient (C_T) for each experiment was one where the voltage measurements ($\Delta \psi$) are taken from locations A and B (Figure 4.2), then are plotted with the change in temperature (ΔT, Figure 4.3), which is the difference in temperature from location A or B ($T_{A\,or\,B}$) to location H (T_H),

$$\Delta T = T_{A\,or\,B} - T_H . \tag{22}$$

This convention is chosen because the reference electrode is always placed at location H and the measuring electrode at the respective location, A or B. Over the course of the experiment, the ΔT magnitude increases in the negative direction, and the measured response from the voltage is captured over time (Figure 4.3). It is important to note that the measurements at locations C, D, E, F, and G are not used in the calculations for the thermoelectric coupling coefficient.

20

4.1.3 Self-potential data corrections

Each step of the electrical potential data corrections will be explicitly discussed. First the electrode tip-to-tip voltage taken before and after each measurement indicates the amount of drift that occurs. This drift is assumed to be linear within the electrodes and is removed by Equation 23,

$$\Delta \psi_{DC} = \Delta \psi_{meas} - \psi_{TT}^{o} + \frac{N\left(\psi_{TT}^{f} - \psi_{TT}^{o}\right)}{N_T + 1}.$$ (23)

Here, $\Delta \psi_{DC}$ is the drift corrected potential, $\Delta \psi_{meas}$ is the measured potential, ψ_{TT}^{o} is the initial tip-to-tip electrode potential and ψ_{TT}^{f} is the final tip-to-tip electrode potential. N is the measurement number, N_T is the total number of measurements. In this study, $N_T = 7$ because there are seven locations (A-G) to sample in one measurement.

Table 4.1 Example calculation of background potential measured by the initial condition measurements. Initial conditions (IC) for different time steps are averaged to obtain a background potential $\Delta \psi_B$.

Location	IC3 (mV)	IC4 (mV)	IC5 (mV)	IC6 (mV)	IC7 (mV)	IC8 (mV)	Average Background potential, $\Delta \psi_B$ (mV)
A	-0.16	-0.15	-0.24	-0.25	-0.34	-0.25	-0.23
B	-0.33	-0.40	-0.28	-0.30	-0.48	-0.20	-0.33
C	-0.39	-0.45	-0.41	-0.35	-0.51	-0.35	-0.41
D	-0.55	-0.50	-0.45	-0.50	-0.55	-0.50	-0.51
E	-0.61	-0.55	-0.59	-0.65	-0.79	-0.65	-0.64
F	-0.68	-0.70	-0.73	-0.70	-0.83	-0.70	-0.72
G	-0.74	-0.75	-0.66	-0.65	-0.76	-0.65	-0.70

After the drift correction is made, the background potential ($\Delta \psi_B$) is removed. The initial condition measurement data are taken for at least one hour, using a ten minute sample interval. The initial condition measurements potential's are averaged for each location over this time period (Table 4.1). The first two initial condition measurements data are not used in this average (Table

4.1), because in many of the experiments these first two initial condition measurements show high variability in reference to the average background for an individual location. This may be due to settling of the sand. The average background potential ($\Delta\psi_B$) is then removed from the drift corrected potential ($\Delta\psi_{DC}$),

$$\Delta\psi_{BC} = \Delta\psi_{DC} - \Delta\psi_B \ . \tag{24}$$
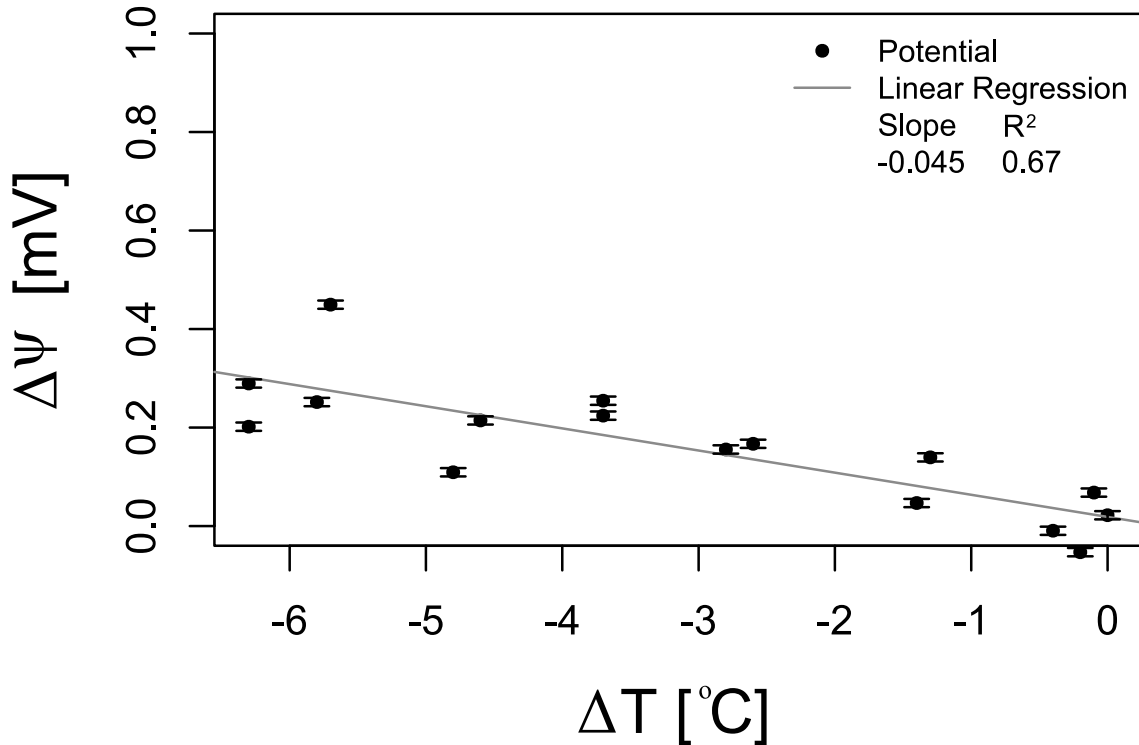
Figure 4.3 Measured potential at locations A and B with a linear regression showing the slope (C_T). This experiment is for a salinity of 0.1 M and sand type 4095. These points have no salinity correction, only background removed. The error bars show the standard error.

The change in temperature (ΔT) versus the background corrected change in potential ($\Delta\psi_{BC}$) can be plotted against one another (Figure 4.4). The slope of the line is the apparent thermoelectric coupling coefficient (C_T) .

Over the course of an experiment, there is a salinity difference that develops across the tank. This salinity gradient is generated as the hot side of the tank's salinity steadily increases in

reference to the cold side, once the temperature begins to rise. Presumably, this increase in salinity is from preferential evaporation on the hot side of the tank over several hours. There are known potential fields that are generated from a salinity gradient (Westerman-Clark and Christoforou, 1986 ,Revil, 1999, Leinov and Jackson, 2014). This self-potential source results from diffusion of ions from regions of high concentration to regions of low concentration within the porous medium and is referred to a diffusion potential (Ikard et al., 2012, Leinov and Jackson, 2014). A voltage correction for the resulting salinity difference must be made.
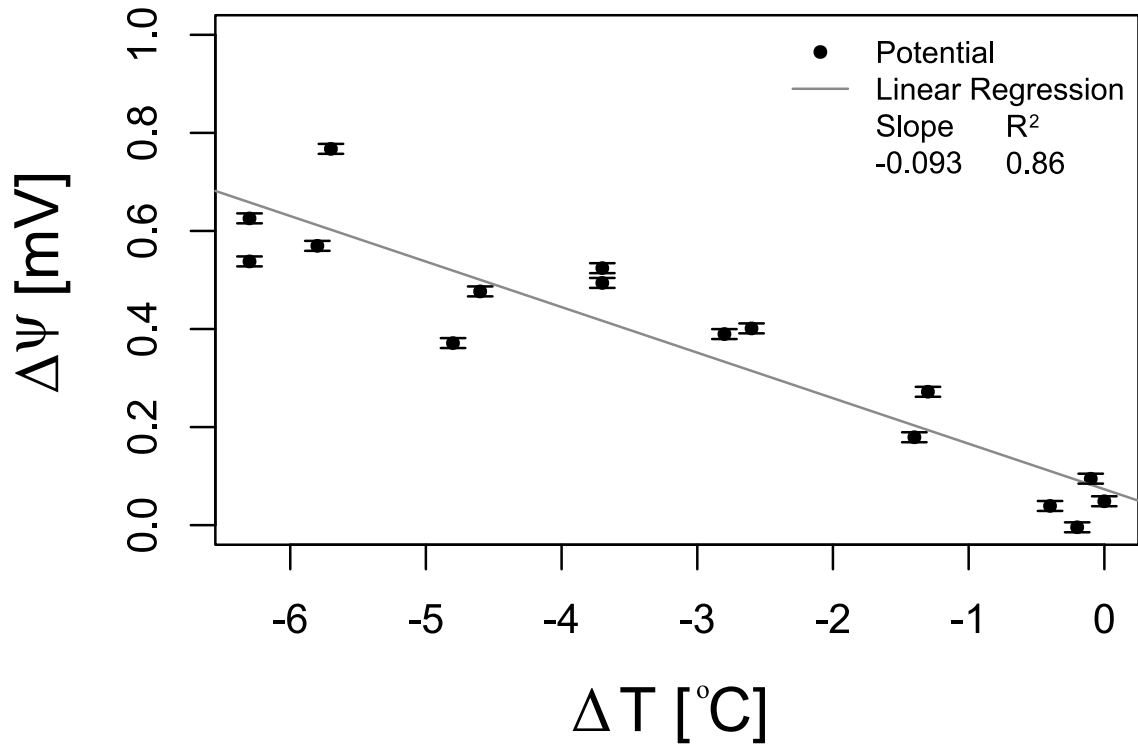
Figure 4.4 Measured potential at locations A and B with a linear regression showing the slope (C_T). This experiment is for a salinity of 0.1 M and sand type 4095 (see Appendix A-2, #9).These points have a salinity correction applied. The slope (C_T) determined here is the value used in Figure 3.1.The error bars show the standard error.

Potentials generated by ion diffusion can be represented by (Revil, 1999),

$$\Delta \psi_{ED} = -\frac{k_B T}{e}\left(2T_{Na}-1\right)\ln\left(\frac{a_H}{a_C}\right).$$ (25)

where a_H and a_C are the activities of the respective hot and cold solutions in the tank.

23

Equation 10 represents electrochemical diffusion at a constant temperature, because this correction will be applied in a non-isothermal system the average temperature between the two measuring locations is used (T_{ave}). The potential generated in this way is subtracted from the corrected potential previously calculated, as shown by,

$$\Delta \psi = \Delta \psi_{BC} - \Delta \psi_{ED}, \tag{26}$$

and,

$$\Delta \psi = \Delta \psi_{BC} + \frac{k_B T_{ave}}{e} (2T_{Na} - 1) \ln \left(\frac{a_H}{a_C} \right). \tag{27}$$

The values used for each term of Equations 26 and 27 are presented in Table 2.1. In order to obtain activities for the corresponding solutions, the Debye and Hückel (1923) solution was used (Domenico and Schwartz, 1997). An example for the differences in salinity-corrected potentials and non-salinity-corrected potentials are shown in Figures 4.3 & 4.4. These corrections become significant at lower salinities.

To determine the macroscopic Hittorf transport number (T_{Na}) for a given experiment the relationships presented in Revil et al. (2008) and Revil and Skold (2011) are used to arrive at Equaiton 15. Data provided by Sakaki (2009) for physical characteristics of the sand (Table 2.2) that are used in all the calculations. The cementation factor *m* is taken to be 1.3, which is reasonable for unconsolidated high silica sands (Revil, 1999). Using these calculations for T_{Na} in each experiment, it is found that the magnitude of the salinity correction increases for low salinities and smaller grain sizes (see equations 13-15).

CHAPTER 5

RESULTS, DISCUSSION AND CONCLUSIONS

An overview of the data is presented. Results are discussed with their relation to the models that are developed. Then the data are compared to other studies.

5.1 Experimental results and discussion

The range of C_T observed for all the samples over the four orders of magnitude of salinity extends from -0.4 to +0.9 (Figure 3.1). There is a trend toward a positive C_T at the lowest salinities tested. At high salinities, both sand grain sizes exhibit low thermoelectric responses of approximately 0 mV/C. There is a general negative C_T trend from high salinity (1 M) to around 10^{-3} M (Figures 3.1, 5.1, 5.2). The two grain sizes tested exhibit noticeably different C_T over the same range of salinity (Figures 3.1, 5.1, 5.2). The finer grained sand (7030) exhibits a greater increase in C_T at the lowest salinities tested, compared to the coarser grained sand (4095). Two experiments in the coarser sand fall outside the range of expected coupling coefficients based on Equations 18 & 21.

The modeled C_T curves based on the salinity and physical parameters of the sand show promise to more accurately predict C_T. The data suggest that the smaller grained sands exhibit a trend toward positive C_T at higher salinities compared to the coarser grained sands (Figure 3.1). In either case, it is shown with these sands that at salinities above 10^{-2} M the C_T approaches 0 mV/C. Salinities below 10^{-2} M have a greater magnitude variation in C_T.

When the experimental data are compared to the models that were created it is clear that there is a strong relationship with one another. This is encouraging for the current models that represent the C_T as ionic diffusion as a result of heating. It is important to note that the Hittorf transport number cannot be taken as a constant when considering the C_T, as discussed in Chapter 3. Ions that could possibly contaminate a solution make it difficult to ensure that relative ion transport numbers are accurate when testing a model. The experimental data for the coarser gained sand within this study did not follow the predicted trend as well as the finer grain sand (Figure 3.1). Taking a closer look at the coarser grained sand, there are visible impurities within this sample

25
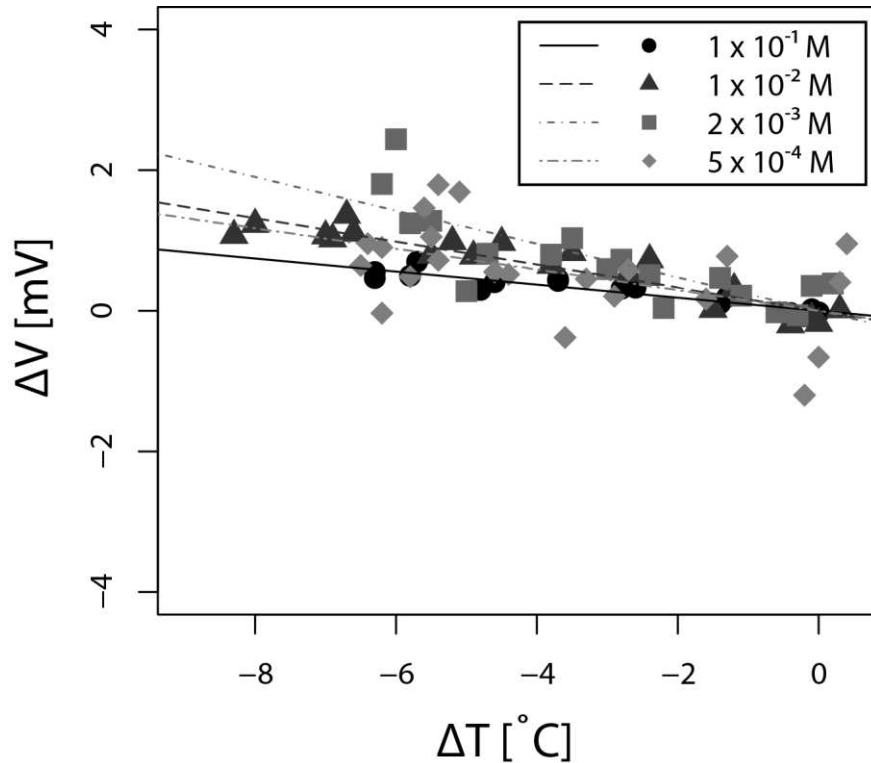
Figure 5.1 Representative experimental data for the coarse grained sand tested (4095). Decreasing salinity with decreasing shade. Approximately one order of magnitude in salinity difference between data sets are represented here. Black circles $(10^{-1}M)$, dark gray triangles $(10^{-2}M)$, grey squares $(10^{-3}M)$, light grey diamonds $(10^{-4}M)$. Linear regression of each experiment is shown, black line $(10^{-1}M)$, dark gray dashed line $(10^{-2}M)$, grey dot-dashed line $(10^{-3}M)$, light grey dot-dashed line $(10^{-4}M)$. Data for experiments can be seen in Appendices A and B.

of silica sand compared to the finer grained sand (Figure 5.3). Impurities such as feldspars and micas are qualitatively present. There is no data from the manufacturer (Unimin Corp.) on specific sands because they mine it in multiple locations, only guaranteeing 87% silica (Unimin Silica Sands MSDS, 2015). The best that can be said is that there is more of a possibility that mineral dissolution from these impurities is possible. The coarse grain model that was developed was unable to take into account these possible differences in the solution chemistry. This is a plausible explanation for C_T observed outside of the theoretical range defined by the bounding Hittorf transport range (Figure 3.1).
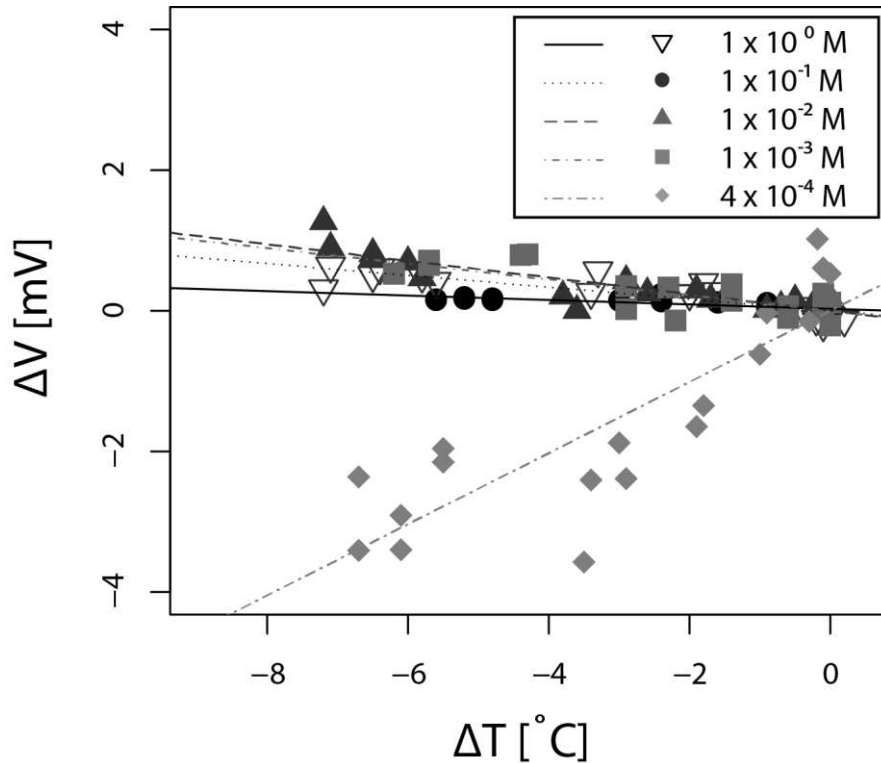
Figure 5.2 Representative experimental data for the fine grained sand tested (7030). Decreasing salinity with decreasing shade. Approximately one order of magnitude in salinity difference between data sets are represented here. Open triangles $(10^0 M)$, black circles $(10^{-1} M)$, dark gray triangles $(10^{-2} M)$, grey squares $(10^{-3} M)$, light grey diamonds $(10^{-4} M)$. Linear regression of each experiment is shown, black line $(10^0 M)$, dotted dark grey $(10^{-1} M)$, dark gray dashed line $(10^{-2} M)$, grey dot-dashed line $(10^{-3} M)$, light grey dot-dashed line $(10^{-4} M)$. Data for experiments can be seen in Appendices A and B.

Convective mixing of the solution within the tank is one other possible source of experimental error that is difficult to predict. An experiment like this one will inevitably have non-uniform horizontal temperature gradients within the tank. This phenomenon was not taken into account within the context of this study.

Observations made from both the HTG and LTG experiments display the same characteristics within the context of the C_T. This observation within the data postulates that the C_T is linear with temperature. The only observed non-linear relationship is C_T with salinity.

The parameter $Q^*_{Na/Cl}$ is known as the single-ion heat of transport. It is used throughout this study within the predictive models for C_T. The heat of transport ($Q^*_{Na/Cl}$ [J mol^{-1}]) refers to the energy state of ions at corresponding temperatures, it can also be referred to as the entropy of transport (Thomas et al., 2012). Essentially this is the amount energy transferred per mol of ions.

Figure 5.3 Photo of the two sand sizes tested. The fine grained sand (7030, left) and the coarser grained sand (4095, right) are pictured.

This parameter is the least understood and least studied of all the parameters used in this paper (Table 2.1). All other parameters used are well studied and commonly accepted within the academic community (Table 2.1). The values of $Q^*_{Na/Cl}$ (Table 2.1) are taken from Agar et al. (1989), one the few studies on the single-ion heat of transport. This parameter could easily be orders of magnitude off from the values published in Agar et al. (1989). The influence of $Q^*_{Na/Cl}$ within the model presented here (Equation 10) essentially shifts the theoretical bounding C_T with Equations 16 and 17. To test what values of $Q^*_{Na/Cl}$ that match the data presented here, it was found that increasing the value of Q^*_{Cl} by one order of magnitude raised the theoretical lower bound of C_T in Equation 16 ($T_{Na} = 0.3962$) to better match what experimental results found in the salinities above 10^{-3} M (Figure 5.4). It is not suggested that the increased value of Q^*_{Cl} is the true value. Just in the consideration of this study, the data were found to match a theoretical C_T where the chloride

ion has approximately an order of magnitude greater ability to transfer heat then previously published in Agar et al (1989).

This study will hopefully be one in many that investigate thermoelectric effects in porous media. The few published articles on this subject leave much to be desired in the conclusions we can draw today. More extreme salinities should be studied as to their effect on C_T. A redesign of this experiment where evaporation off the top of the tank is better regulated would be desirable. Also, a redesigned experiment similar to Ikard and Revil (2014) where the temperature
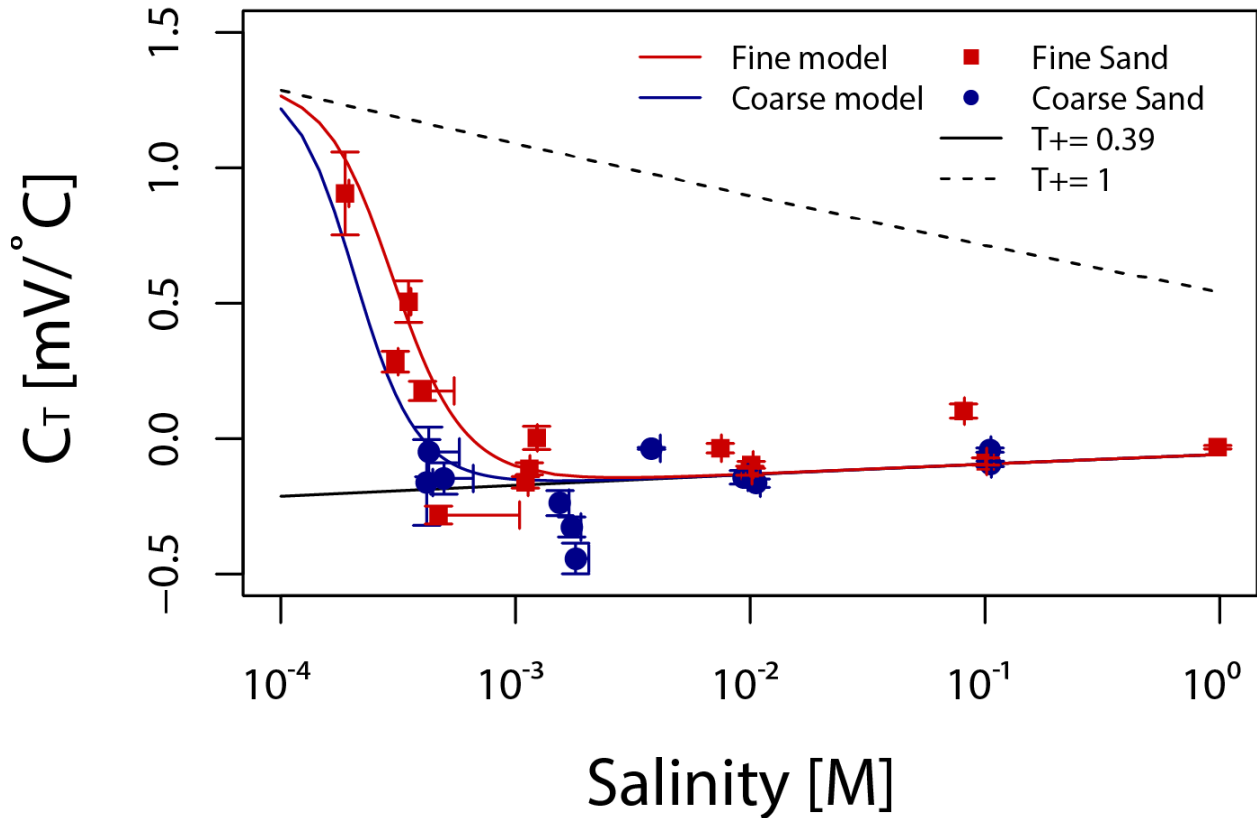
Figure 5.4 Measured thermoelectric response (mV/C) over four orders of magnitude salinity (M). Red squares indicate the fine (7030) type sand, blue circles indicate the course (4095) sand. Adapted model curves are generated with a calculated surface conductivity (σ_s) and formation factor (F) using Equation 18 and a Q_{Cl}^* of 5.3 KJ mol^{-1}, ten times the reported value in Agar et al. (1989). The solid black theoretical C_T bounding line is generated through Equation 18 where $T_{NA/+} = 0.3962$. The dotted black line represents Equaiton 21 where $T_{NA/+} = 1$. The error in experimental measurenets is reported as residual standard error. Data presented here are discussed in Chapter 4 and in Appendicies A an B.

contamination of the electrodes is eliminated, so that a better estimate of C_T is made, could prove highly valuable in the continued effort to reveal the underlying physics this subject of study.

An effort is currently being made in Dr. André Revil's group of students at Colorado School of Mines to continue these experiments for a sandstone that is known to have a high surface conductivity. A high surface conductivity media is predicted to have a higher T_{Na} at higher salinities in comparison to lower surface conductivity media (Section 2.1.1). The data from this experiment will be compared to the model that is created in this paper to predict C_T with various material properties. The model's prediction for this sandstone will be one where the C_T trends positive at much higher salinities in comparison to the one here.

5.2 Conclusions

The following conclusions have been reached:

(1) The thermocoupling coefficient C_T in saturated unconsolidated silica sand varies according to salinity and grain size and was observed to range from -0.4 to 0.9 over four orders of magnitude in NaCl electrolyte tested. Grain diameter and salinity controlled modeled C_T response from negative to positive in a predictable way.

(2) The magnitude of the thermocoupling coefficient C_T increases positively at salinities below 10^{-3} M NaCl and trends toward zero at higher salinities.

(3) Salinity gradients generated from a small amount of preferential evaporation must be taken into account when investigating C_T. These spurious effects as well as those associated with the temperature dependence of the electrodes themselves should be controlled with care in order to have reliable measurements.

REFERENCES CITED

[1] Abaza, M. M. I., and C. G. Clyde, 1969, Evaluation of the rate of flow through porous media using electrokinetic phenomena: Water Resources Research, **5**, 470-483.

[2] Agar, J. N., C. Y. Mou, and J. L. Lin, 1989, Single-ion heat of transport in electrolyte solutions: a hydrodynamic theory: The Journal of Physical Chemistry**, 93,** 2079–2082.

[3] Archie, G. E., 1942, The electrical resistivity log as an aid in determining some reservoir characteristics: Transactions of the Am. Inst. Min. Metall. Pet. Eng., **146**, 54-62.

[4] Corwin, R. F. and D. B. Hoover, 1979, The self-potential method in geothermal exploration. Geophysics, **44,** 226–245.

[5] Domenico, P.A., and F.W. Schwartz, 1997, Physical and Chemical Hydrogeology, 2nd Edition, Wiley, 506.

[6] Johnson Controls, Accessed May 2015, Electronic temperature control, http://www.johnsoncontrols.com.

[7] Goodwin, H. M., M. Harry, M. Faraday, J. W. Hittorf and F. W. G.Kohlrausch, 1899, The fundamental laws of electrolytic conduction; memoirs by Faraday, Hittorf and F. Kohlrausch. New York, London, Harper & brothers.

[8] Gulamali, M. Y., E. Leinov, and M.D. Jackson, 2011, Self-potential anomalies induced by water injection into hydrocarbon reservoirs, Geophysics, **76,** F283–F292.

[9] Ikard, S. J., A. Revil, A. Jardani, W. F. Woodruff, M. Parekh, and M. Mooney, 2012, Saline pulse test monitoring with the self-potential method to non-intrusively determine the velocity of the pore water in leaking areas of earth dams and embankments: Water Resources Research, **48**, W04201, doi:10.1029/2010WR010247.

[10] Ikard, S. J., and A. Revil, 2014, Self-potential monitoring of a thermal pulse advecting through a preferential flow path: Journal of Hydrology: **519**, A, 34-49, doi: 10.1016/j.jhydrol.2014.07.001.

[11] Jougnot, D., N. Linde, E. B. Haarder and M. C. Looms, 2015,Monitoring of saline tracer movement with vertically distributed self-potential measurements at the HOBE agricultural test site, Voulund, Denmark. Journal of Hydrology **521,** 314–327.

[12] Karaoulis, M., A. Revil, and D. Mao, 2014, Localization of a coal seam fire using combined self-potential and resistivity data: International Journal of Coal Geology, **128-129**, 109-118, doi: 10.1016/j.coal.2014.04.011.

[13] Leinov, E., J. Vinogradov, and M. D. Jackson, 2010, Salinity dependence of the thermoelectric coupling coefficient in brine-saturated sandstones: Geophysical Research Letters, **37**, L23308, doi:10.1029/2010GL045379.

[14] Leinov, E., and M. D. Jackson, 2014, Experimental measurements of the SP response to concentration and temperature gradients in sandstones with application to subsurface geophysical monitoring. Journal of Geophysical Research, **119,** 2014JB011249.

[15] Levy, A. L., 1952, Difficulties in the Hittorf method of determining transference numbers. *J. Chem. Educ.* **29,** 384.

[16] Lide, D. R., 2009, CRC Handbook of Chemistry and Physics, 89th ed., CRC Press, Taylor and Francis, Boca Raton, FL, ISBN 142006679X.

[17] Marshall, D. J. and T. R. Madden, 1959,Induced polarization, a study of its causes. Geophysics **24,** 790–816.

[18] Meyer, C. and A .Revil, Submitted 2015. A Laboratory investigation of the thermoelectric effect in clean sands. Geophysics. GEO-2015-0281.

[19] Negi, A. S. and S. C. Anand, 1985,A Textbook of Physical Chemistry. New Age International.

[20] Nightingale, E. R., 1959, Phenomenological Theory of Ion Solvation. Effective Radii of Hydrated Ions. J. Phys. Chem. **63,** 1381–1387.

[21] Nourbehecht, B., 1963, Irreversible thermodynamics effects in inhomogeneous media and their applications in certain geoelectric problems: Ph.D. thesis, Mass Inst. of Technol., Cambridge, Mass.

[22] Petiau, G., 2000, Second generation of lead-lead chloride electrodes for geophysical applications: Pure and Applied Geophysics, **157**, 357– 382.

[23] Revil, A., 1999, Ionic diffusivity, electrical conductivity, membrane and thermoelectric potentials in colloids and granular porous media: a unified model: Journal of Colloid and Interface Science, **212**, 503-522.

[24] Revil, A., N. Florsch and C. Camerlynck, 2014, Spectral induced polarization porosimetry. Geophys. J. Int. **198,** 1016–1033.

[25] Revil, A., L. M. Cathles, S. Losh, and J.A. Nunn, 1998, Electrical conductivity in shaly sands with geophysical applications: Journal of Geophysical Research, **103,** 23925–23936.

[26] Revil, A., and N. Florsch, 2010, Determination of permeability from spectral induced polarization data in granular media: Geophysical Journal International, **181**, 1480-1498, doi: 10.1111/j.1365-246X.2010.04573.x.

[27] Revil, A. and D. Jougnot, 2008, Diffusion of ions in unsaturated porous materials. J Colloid Interface Sci 319, 226–235.

[28] Revil, A. and H. Mahardika, 2013, Coupled hydromechanical and electromagnetic disturbances in unsaturated porous materials. Water Resour. Res. **49,** 744–766.

[29] Revil, A., and M. Skold, 2011, Salinity dependence of spectral induced polarization in sands and sandstones, Geophysical Journal International, **187,** 813–824.

[30] Revil, A., M. Karaoulis, S. Srivastava, and S. Byrdina, 2013, Thermoelectric self-potential and resistivity data localize the burning front of underground coal fires: Geophysics, **78**, no. 5, B259–B273.

[31] Risgaard-Petersen, N., A. Revil, P. Meister, and L.P. Nielsen, 2012, Sulfur, iron-, and calcium cycling associated with natural electric currents running through marine sediment: Geochimica et Cosmochimica Acta, **92**, 1–13.

[32] Rittgers, J. B., A. Revil, M. Karaoulis, M. A. Mooney, L.D. Slater, and E.A. Atekwana, 2013, Self-potential signals generated by the corrosion of buried metallic objects with application to contaminant plumes: Geophysics, **78,** EN65–EN82.

[33] Sakaki, T., 2009, Physical, hydraulic, and thermal properties of silica sands for laboratory experiments. Internal Report, Center for Experimental Study of Subsurface Environmental Processes (CESEP), Colorado School of Mines, Golden, Colorado.

[34] Stern, O., 1924. Zur Theorie der elektrolytischen Doppelschicht (The theory of the electrolytic double shift). Zeitschrift Fur Elektrochemie Und Angewandte Physikalische Chemie, 30, 508-516.

[35] Tasaka, M., S. Morita, and M. Nagasawa, 1965, Membrane potential in nonisothermal systems: Journal of Physical Chemistry, **69**, 4191–4197.

[36] Thomas, H. R., M. Sedighi, and P. J. Vardon, 2012, Diffusive Reactive Transport of Multicomponent Chemicals Under Coupled Thermal, Hydraulic, Chemical and Mechanical Conditions. Geotech Geol Eng **30,** 841–857.

[37] Unimin Silica Sand MSDS. Accessed May 2015. Crystalline silica from Quartz [Materials Safety Data Sheet]. http://www.unimin.com/

[38] Valkenburg, M.E.V., Vaughn, R.L., M. Williams, and J. S. Wilkes, 2005, Thermochemistry of ionic liquid heat-transfer fluids. Thermochimica Acta **425,** 181–188.

[39] Vigolo, D., S. Buzzaccaro, and R. Piazza, 2010, Thermophoresis and Thermoelectricity in Surfactant Solutions. Langmuir **26,** 7792–7801.

[40] Westermann-Clark, G. B. and C.C. Christoforou, 1986, The exclusion-diffusion potential in charged porous membranes: Journal of Electroanalytical Chemistry and Interfacial Electrochemistry, **198**, 213–231.

APPENDIX A

COURSE GRAIN EXPERIMENT DATA AND STATISTICS

Table A-1 Coarse grained sand (4095) experimental data showing measured data, regression of slope in Table A-2, standard calculated error, and calculated macroscopic Hittorf number for each experiment. This data corresponds to data presented in Table A-2.

Experiment #	Salinity (M)	R^2	C_T (mV/°C)	Standard Error Voltage (mV)	Standard Error Salinity (M)	Standard Error Slope	T+
1	4.19E-04	0.06	-1.62E-01	1.65E+00	2.53E-05	1.58E-01	0.47
2	4.27E-04	0.02	-4.88E-02	1.03E+00	1.50E-04	9.17E-02	0.47
3	4.96E-04	0.24	-1.47E-01	6.30E-01	1.65E-04	5.79E-02	0.45
4	1.55E-03	0.62	-2.38E-01	4.14E-01	1.44E-04	4.63E-02	0.40
5	1.73E-03	0.81	-3.26E-01	3.83E-01	1.65E-04	3.69E-02	0.40
6	1.80E-03	0.77	-4.42E-01	6.30E-01	2.49E-04	5.69E-02	0.40
7	3.79E-03	0.88	-3.57E-02	1.91E-01	3.45E-04	3.53E-03	0.40
8	9.36E-03	0.67	-1.43E-01	2.89E-01	4.17E-04	2.49E-02	0.40
9	1.06E-02	0.87	-1.64E-01	1.87E-01	4.41E-04	1.52E-02	0.40
10	1.05E-01	0.64	-4.21E-02	1.00E-01	9.89E-04	7.87E-03	0.40
11	1.05E-01	0.86	-9.29E-02	9.13E-02	1.13E-03	1.01E-02	0.40

Table A-2 Coarse grained sand (4095) experimental data showing temperature and voltage measurements. Each experiment number corresponds to other data presented in Appendix A-1. Each of these experiments are corrected for salinity differences that arose during the data collection. Salinity data shown here are referenced from the starting salinity of the experiment.

#1		#2		#3		#4		#5		#6	
Salinity (M)	4.19E-04	Salinity (M)	4.27E-04	Salinity (M)	4.96E-04	Salinity (M)	1.55E-03	Salinity (M)	1.73E-03	Salinity (M)	1.80E-03
delta V (mV)	delta T (°C)	delta V (mV)	delta T (°C)	delta V (mV)	delta T (°C)	delta V (mV)	delta T (°C)	delta V (mV)	delta T (°C)	delta V (mV)	delta T (°C)
-0.17	-0.40	0.75	-0.10	0.62	0.30	0.83	-0.10	0.23	-0.10	-0.49	0.00
0.64	-0.90	0.85	-0.60	-0.98	-0.20	0.46	-0.60	0.60	-0.20	0.15	-0.30
0.31	-1.80	0.93	-1.50	0.38	-1.60	0.95	-1.40	0.12	-0.90	-0.24	-1.10
-2.90	-3.10	-1.68	-2.60	0.42	-2.90	0.99	-2.40	0.73	-1.60	-0.06	-3.00
-1.72	-4.40	-0.86	-3.80	-0.16	-3.60	1.07	-3.00	0.24	-2.70	-0.06	-2.50
1.92	-4.60	-0.02	-4.10	0.77	-4.60	1.28	-3.80	0.83	-3.30	0.28	-4.30
-3.04	-6.90	0.58	-6.40	0.93	-5.40	0.76	-5.00	1.06	-4.10	0.17	-3.70
3.19	-6.80	-0.72	-7.40	0.70	-5.80	1.73	-5.80	1.46	-5.30	2.36	-5.50
0.55	-7.00	-0.71	-7.50	1.27	-5.50	2.28	-6.20	2.33	-6.10	2.59	-6.30
-0.26	-0.10	-1.46	0.00	0.18	-6.20	0.87	0.20	2.54	-6.90	2.72	-8.00
-1.00	-0.60	-1.00	-0.30	0.86	-6.50	0.42	-0.30	0.51	0.20	-0.49	0.20
-1.74	-1.60	1.11	-1.20	1.17	0.40	0.70	-1.10	0.51	0.00	0.16	-0.08
-1.12	-3.00	-0.59	-2.50	-0.44	0.00	0.52	-2.20	0.23	-0.60	-0.22	-0.90
-1.76	-4.40	0.80	-3.60	0.99	-1.30	1.21	-2.80	0.55	-1.40	-0.45	-2.80
0.82	-4.40	0.61	-3.70	0.80	-2.70	1.51	-3.50	0.24	-2.40	0.16	-2.30
-0.06	-6.60	0.13	-6.20	0.67	-3.30	1.29	-4.70	0.83	-3.00	0.17	-4.00
1.22	-6.40	2.13	-7.10	0.73	-4.40	1.76	-5.50	1.27	-3.90	0.61	-3.50
1.09	-6.80	0.39	-7.20	1.91	-5.10	2.92	-6.00	1.97	-5.00	2.19	-5.20
				1.68	-5.60			2.54	-5.80	2.70	-5.90
				2.01	-5.40			2.53	-6.60	3.13	-7.70
				1.12	-6.20						
				1.17	-6.40						

36

Table A-3 Continued

	#7		#8		#9		#10		#11
Salinity (M)	3.79E-03	Salinity (M)	9.36E-03	Salinity (M)	1.06E-02	Salinity (M)	1.05E-01	Salinity (M)	1.05E-01
delta V (mV)	delta T (°C)	delta V (mV)	delta T (°C)	delta V (mV)	delta T (°C)	delta V (mV)	delta T (°C)	delta V (mV)	delta T (°C)
0.31	-0.20	0.07	-0.40	-0.12	0.00	0.10	-0.10	0.09	-0.10
0.38	-1.90	0.16	-0.90	-0.14	-0.40	0.03	-0.70	0.04	-0.40
0.93	-4.30	0.27	-2.40	0.08	-1.50	0.12	-2.00	0.18	-1.40
0.85	-8.10	0.05	-3.70	0.59	-2.70	0.14	-4.40	0.39	-2.80
0.91	-12.70	0.02	-5.30	0.70	-3.80	0.40	-4.80	0.49	-3.70
1.15	-17.80	0.44	-5.90	0.83	-4.90	0.27	-6.10	0.37	-4.80
1.55	-30.80	0.90	-7.40	0.85	-5.50	0.50	-7.60	0.57	-5.80
2.07	-40.20	1.24	-7.60	1.08	-6.90	0.43	-8.20	0.54	-6.30
0.66	0.00	1.28	-8.00	1.12	-7.00	0.29	-8.50	0.05	0.00
0.65	-1.60	0.11	-0.30	1.13	-8.30	0.05	0.10	0.00	-0.20
0.72	-3.90	0.36	-1.00	0.07	0.30	0.11	-0.50	0.27	-1.30
1.12	-7.90	0.39	-2.40	-0.05	-0.10	0.19	-1.70	0.40	-2.60
1.27	-12.70	0.28	-3.70	0.37	-1.20	0.20	-4.10	0.52	-3.70
1.51	-17.60	0.35	-5.30	0.78	-2.40	0.36	-4.60	0.48	-4.60
1.83	-30.70	0.76	-5.90	0.88	-3.50	0.40	-5.80	0.77	-5.70
1.83	-40.30	0.93	-7.30	1.03	-4.50	0.53	-7.30	0.63	-6.30
		1.26	-7.60	1.04	-5.20	0.49	-7.90		
		1.50	-8.00	1.16	-6.60	0.22	-8.20		
				1.42	-6.70				
				1.29	-8.00				

FINE GRAIN EXPERIMENT DATA AND STATISTICS

Table B-1 Fine grained sand (7030) experimental data showing measured data, regression of slope in Table B-2, standard calculated error, and calculated macroscopic Hittorf number for each experiment. This data corresponds to data presented in Table B-2.

Experiment #	Salinity (M)	R^2	C_T (mV/°C)	Standard Error Voltage (mV)	Standard Error Salinity (M)	Standard Error Slope	T+
1	1.88E-04	0.74	9.06E-01	8.31E-01	7.33E-06	1.53E-01	0.92
2	3.08E-04	0.77	2.84E-01	4.18E-01	8.60E-06	3.84E-02	0.73
3	3.50E-04	0.73	5.06E-01	7.77E-01	8.06E-06	7.66E-02	0.67
4	4.02E-04	0.61	1.76E-01	2.23E+00	1.46E-04	3.55E-02	0.61
5	4.70E-04	0.80	-2.82E-01	1.82E+00	5.70E-04	3.30E-02	0.56
6	1.10E-03	0.78	-1.61E-01	9.40E-01	2.88E-05	2.14E-02	0.42
7	1.15E-03	0.61	-1.11E-01	2.08E-01	6.98E-06	2.21E-02	0.42
8	1.23E-03	0.00	3.05E-03	3.72E-01	6.98E-06	4.29E-02	0.42
9	7.45E-03	0.22	-3.50E-02	6.21E-01	7.85E-05	1.76E-02	0.40
10	9.96E-03	0.76	-1.18E-01	1.84E-01	2.14E-04	1.68E-02	0.40
11	1.01E-02	0.78	-9.65E-02	1.35E-01	1.95E-04	1.28E-02	0.40
12	8.10E-02	0.46	1.02E-01	1.40E+00	7.36E-04	2.62E-02	0.40
13	1.01E-01	0.71	-8.38E-02	1.49E-01	1.12E-03	1.33E-02	0.40
14	9.79E-01	0.59	-3.14E-02	5.61E-02	2.42E-03	6.50E-03	0.40

Table B-2 Fine grained sand (7030) experimental data showing temperature and voltage measurements. Each experiment number corresponds to other data presented in Appendix B-1. Each of these experiments are corraected for salinity differences that arose during the data collection. Salinity data shown here are referenced from the starting salinity of the experiment.

#1		#2		#3		#4		#5		#6	
Salinity (M)	1.88E-04	Salinity (M)	3.08E-04	Salinity (M)	3.50E-04	Salinity (M)	4.02E-04	Salinity (M)	4.70E-04	Salinity (M)	1.10E-03
delta V (mV)	delta T (°C)	delta V (mV)	delta T (°C)	delta V (mV)	delta T (°C)	delta V (mV)	delta T (°C)	delta V (mV)	delta T (°C)	delta V (mV)	delta T (°C)
-3.94	-0.20	-0.05	0.00	-0.10	-0.10	-1.30	-0.60	0.26	-0.50	0.74	0.00
-1.43	-0.30	-0.92	-0.30	-0.86	-0.30	-2.18	-1.00	-1.76	-1.60	1.03	-0.30
-3.36	-1.50	-0.76	-0.60	-1.32	-1.00	-2.64	-3.00	-1.92	-3.70	2.42	-1.50
-3.24	-2.10	-1.52	-1.70	-2.35	-1.90	-4.38	-6.40	-0.61	-8.50	2.92	-3.50
-5.00	-2.90	-1.95	-2.70	-2.58	-3.00	-6.46	-10.30	-0.70	-12.50	3.37	-6.40
-5.23	-3.20	-1.86	-3.60	-4.28	-3.50	-9.17	-14.40	-0.97	-13.70	3.31	-10.40
-6.63	-4.40	-2.23	-4.90	-2.67	-5.50	-9.50	-25.10	-1.05	-18.80	3.42	-17.70
-3.78	0.00	-2.78	-6.50	-4.10	-6.10	-10.92	-37.50	6.54	-26.90	3.81	-25.40
-1.85	-0.10	-1.99	-7.30	-4.11	-6.70	-7.01	-41.90	7.04	-34.10	6.28	-28.70
-3.09	-1.30	-0.13	0.20	-0.18	0.00	-1.32	-0.20	7.57	-36.30	0.64	0.00
-3.37	-1.90	-1.19	-0.10	0.26	-0.20	-2.20	-0.70	-0.11	-0.30	1.25	-0.30
-5.45	-2.70	-0.69	-0.50	-0.74	-0.90	-2.99	-2.60	-1.02	-1.40	2.25	-1.40
-4.97	-3.10	-1.72	-1.50	-2.05	-1.80	-4.74	-6.00	-0.69	-3.60	2.62	-3.30
-6.60	-4.30	-1.70	-2.50	-3.09	-2.90	-6.60	-10.20	0.24	-8.40	3.89	-6.20
		-2.10	-3.40	-3.11	-3.40	-9.91	-14.10	0.57	-12.40	4.66	-10.30
		-2.11	-4.80	-2.86	-5.50	-9.19	-24.90	0.34	-13.50	5.30	-17.60
		-3.03	-6.50	-3.61	-6.10	-11.50	-37.20	-0.14	-18.60	5.97	-25.20
		-2.55	-7.10	-3.07	-6.70	-7.27	-41.60	6.62	-26.70	7.35	-28.60
								8.77	-33.70		
								9.77	-35.90		

Table B-3 Continued

#7		#8		#9		#10		#11		#12	
Salinity (M)	1.15E-03	Salinity (M)	1.23E-03	Salinity (M)	7.45E-03	Salinity (M)	9.96E-03	Salinity (M)	1.01E-02	Salinity (M)	8.10E-02
delta V (mV)	delta T (°C)	delta V (mV)	delta T (°C)	delta V (mV)	delta T (°C)	delta V (mV)	delta T (°C)	delta V (mV)	delta T (°C)	delta V (mV)	delta T (°C)
0.34	-0.10	0.04	0.00	0.56	-0.20	-0.12	-0.20	0.02	0.00	-0.38	-0.30
0.21	0.00	0.02	-0.30	0.45	-1.10	-0.11	-0.50	-0.25	-0.10	0.44	-1.00
0.16	-0.60	0.15	-0.70	0.02	-3.20	-0.24	-0.90	-0.07	-0.30	0.70	-3.40
0.47	-1.40	-0.03	-1.50	1.02	-6.10	0.03	-1.90	-0.08	-0.80	1.04	-6.40
0.42	-2.30	-0.34	-3.00	1.21	-9.40	0.16	-2.90	-0.06	-1.40	0.51	-9.20
0.44	-2.90	-0.13	-3.60	1.73	-11.90	-0.06	-3.80	0.18	-3.20	0.20	-12.80
0.89	-4.40	0.19	-3.90	0.93	-20.40	0.43	-6.00	0.39	-4.80	1.58	-16.90
0.81	-5.70	0.35	-5.10	0.81	-26.70	0.55	-6.50	0.35	-5.80	1.26	-25.50
0.62	-6.20	0.21	-6.20	0.23	-0.30	1.00	-7.20	0.71	-6.70	-2.13	-30.70
-0.12	0.00	0.01	-0.20	0.56	-1.20	-0.09	0.00	0.18	0.10	-3.91	-35.00
0.11	-0.10	0.08	-0.40	0.96	-3.40	-0.20	-0.20	0.10	0.10	0.21	-0.20
-0.01	-0.60	0.10	-0.80	1.31	-6.10	-0.20	-0.70	0.07	-0.10	0.52	-0.80
0.24	-1.40	-0.26	-1.60	2.24	-9.60	-0.10	-1.70	0.06	-0.60	0.73	-3.00
-0.04	-2.20	-0.62	-3.10	2.24	-11.80	-0.01	-2.60	0.14	-1.30	1.57	-5.90
0.12	-2.90	-1.06	-3.70	1.87	-20.50	-0.26	-3.60	0.17	-3.00	1.59	-9.00
0.90	-4.30	0.07	-3.90	1.54	-26.50	0.21	-5.80	0.62	-4.70	1.32	-12.70
0.74	-5.70	0.44	-5.10			0.49	-6.50	0.48	-5.70	1.87	-16.80
0.62	-6.20	-0.35	-6.10			0.64	-7.10	0.71	-6.60	0.18	-25.20
										-2.96	-30.70
										-4.29	-34.70

Table B-4 Continued

	#13		#14
Salinity (M)	1.01E-01	Salinity (M)	9.79E-01
delta V (mV)	delta T (°C)	delta V (mV)	delta T (°C)
-0.01	-0.10	-0.06	0.00
0.07	-0.20	0.00	-0.20
0.19	-0.60	0.12	-0.90
0.43	-2.00	0.11	-1.60
0.43	-2.00	0.13	-2.40
0.44	-3.40	0.14	-3.00
0.68	-5.80	0.15	-4.80
0.69	-6.50	0.17	-5.20
0.50	-7.20	0.15	-5.60
0.05	0.20	-0.05	0.00
0.10	0.00	0.02	-0.20
0.24	-0.40	0.04	-0.90
0.46	-1.70	0.12	-1.60
0.59	-1.80	0.24	-2.40
0.75	-3.30	0.16	-3.00
0.60	-5.60	0.18	-4.80
0.79	-6.40	0.19	-5.20
0.82	-7.10	0.16	-5.60